Università degli Studi di Padova

Department of Information Engineering

Master Thesis in Automation Engineering

Feedforward control of an active seat for dynamic driving simulators

Supervisor
Prof. Ing. Alessandro Beghi
Università di Padova

Co-supervisor
Ing. Mattia Bruschetta
Università di Padova

Master Candidate
Riccardo Dal Borgo

14 October 2019 - Academic Year 2019/2020

Abstract

Dynamic driving simulators are nowadays a common tool in the automotive industry. Due to the simulator physical limitations, the inertial stimulation is subjected to missing cues, false cues and/or scaling errors, decreasing the realism of the simulation. The Active Seat (AS) system is a promising solution to overcome the lacking of low-frequency sustained accelerations. The AS system provides artificial pressure cues to cheat the driver's sensory system to perceive an increased acceleration. This is possible since, in the human brain, the motion perception is the result of a a multisensory integration of different sensory systems. The open problem is how to compute these pressure cues to achieve the best driving simulation experience. Two different ways are explored: the perfect reproduction of the pressure stimuli of a real vehicle or the creation of an haptic feedback to transmit information on the acceleration vector. In this work, the control schemes are developed and analyzed for both approaches. All control schemes developed take into account the pressure induced by the platform movement and achieve good results in the computation of the AS control signals. A test on a real platform and a professional driver will be needed to assert which of the two different control strategies ensure a better experience. For the evaluation of the pressure between the driver and the seat, a nonlinear model of a seated driver subjected to acceleration is introduced.

Sommario

Al giorno d'oggi i simulatori di guida dinamici sono sempre più comuni nel settore automobilistico. I limiti fisici della piattaforma comportano stimolazioni errate, mancanti o riscalate durante il movimento, diminuendo il realismo della simulazione. Il systema Active Seat (AS) è una soluzione promettente per compensare la mancanza delle componenti di acclereazione a bassa frequenza o sostenute nel tempo. Il sistema AS fornisce degli stimoli pressori artificiali per far percepire al pilota delle accelerazioni più intense. Tale fenomeno è possibile in quanto la percezione del movimento nell'essere umano è il risultato dell'integrazione di vari stimoli originati da diversi sistemi percettivi. Rimane una questione aperta quale sia la strategia migliore per generare tali stimoli pressori affinché sia massimizzato il realismo della simulazione. In questa tesi sono analizzate due diverse strategie: la riproduzione esatta degi stimoli pressori che si percepirebbero alla guida di una macchina vera o la trasmissione di un informazione più semplice, legata al vettore accelerazione, sottoforma di feeback aptico. In questo elaborato vengono sviluppati ed analizzati gli schemi di controllo per entrambe le strategie, tenendo in considerazione il contributo pressorio indotto dal movimento della piattaforma stessa. I risultati ottenuti sono buoni per tutti gli schemi di controllo proposti. La miglior strategia di controllo per l'AS sarà individuata in un futuro test in piattaforma con un pilota professionista. Per la valutazione della pressione è stato introdotto un modello non lineare del corpo del pilota soggetto ad accelerazioni esterne.

Contents

1 Introduction

In recent years, driving simulators are an important topic in the automotive field. The interest in this technology is due to the wide range of possible applications in which they are used. Initially the driving simulators were developed for driver's training in the racing area, however, nowadays, they are used both in R&D and production departments. They are great tools for the development of autonomous driving systems and advanced driving assistance systems (ADAS). In a simulator platform, human-machine interactions can be analyzed in a safe and repeatable way, also in rare or dangerous road scenarios. The driving simulators can be roughly divided in two macro categories: static simulators where the seat is fixed on the ground, the driver receives only visual and auditory cues, and dynamic simulators, where the platform movement add the inertial stimulation of the driver. In the dynamic case, a critical role is played by the Motion Cueing Algorithms (MCAs). The fidelity of the reproduction of the driving feeling of the real car is strongly characterized by the simulator capability of reproduce the inertial stimuli on the driver. The classical MCAs are based on a combination of high-pass and low-pass filters, focusing on the reproduction of the high-frequency components. The low-frequency dynamics is reproduced by down-scaling and tilt coordination, trying not to compromise the realism of the motion cues while reducing the actual platform movement and the distance from its neutral position [1]. In most cases, the physical constraints of the platform preclude a 1:1 reproduction of the desired accelerations. The modern MCAs exploit model predictive control (MPC) to achieve better performance and to optimize the coverage of the available workspace [2], [3], [4]. Although these improve-

ments, the MCAs cannot entirely prevent missing cues, false cues, and scaling errors. These artifacts, in the simulator dynamics, can decrease the realism of the simulation and also can cause motion sickness [1].
To overcome these limitations, other sensory cues must be considered to enrich the simulated experience. The perception of motion in the human being is the overall result of the cooperation of the visual, auditory, tactile, and vestibular systems. The main contribution, besides the visual stimuli, is given by the vestibular system formed by the semicircular canals and ootholits of the inner ear, which are responsible for the perception of the angular and linear accelerations. The somatosensory system, composed by various sensory neurons throughout the body, has also an important role since the pressure cues, if coordinated with the stimuli from other senses, are used for the perception of self-motion and spatial orientation. In the neuroscientific literature is well established that the human brain constructs a unified conscious experience from multisensory cues. The most accredited theory is that the human brain creates a robust percept of the external environment by integrating multiple sensory information in a statistically optimal way [5],[6]. In the dynamic simulators, this fact can be exploited by artificially recreate pressure cues on the driver's body to trick the driver's sensory system to perceive an higher acceleration. For this purpose the Active Seat technology can be used to provide pressure on specific areas of the driver's body and reproduce the feeling of the low-frequency sustained accelerations that are usually lacking in simulators with limited workspace. The effectiveness of the Active Seat system and its artificial pressure cues is proven in [7], but how to compute the best pressure cues between the Active Seat and the driver's body is still an open problem. There are in fact two possible different strategies:

- *The haptic feedback strategy*: the pressure cues are computed to transmit to the driver an information directly connected to the actual acceleration and its direction.
- *Model-based pressure cues*: the pressure cues aim at recreating the same pressure cues the driver would feel in the real car, taking into account the driver's dynamic on the seat.

The goal of this thesis is to develop and analyze the control strategies for both approaches. This study is a preliminary work for a test in a real simulator with a professional driver. In the control strategies proposed in this thesis, the pressure induced on the driver's body by the movement of the simulator platform is taken into account. For the model-based pressure cues approach, a nonlinear model of a seated driver is introduced and further developed to achieve the desired performance. This model allows to consider the driver's dynamics in

the pressure computation, both in a real vehicle and in the simulator. Two different control schemes are proposed, one based on a feedforward scheme and one based on the MPC scheme.
For the haptic feedback approach instead, two different models are introduced where the driver's dynamic on the seat is not take into account. This allows to compute a pressure directly connected to the acceleration signals. These two models are then exploited in two different control schemes: one is a slightly modified version of the actual control system and one based on the feedforward control.
In details, the thesis is organized as follow:

- *Chapter 2* starts with the presentation of the Active Seat system and its actual control scheme with an haptic feedback strategy. In the second part, the lateral pressure model of the driver and the model of the Active Seat bladders are introduced.
- *Chapter 3* describes an enhanced version of the lateral pressure model of the driver. In the second part, a feedforward control scheme and Model Predictive Control strategy are developed, both embodying the model-based pressure cue approach.
- *Chapter 4* presents an enhanced version of the actual control to obtain an haptic feedback.
- *Chapter 5* shows the results of the proposed control schemes for both strategies.
- *Chapter 6* provides a summary of the work and concluding remarks are given. Finally, some considerations on possible future investigations are made.

2

Active Seat system and algorithms: state of the art

At the start of this chapter, the active seat system is described. Moreover, in section 2.2, the actual control scheme is illustrated as reported in the VI-DriveSim documentation [8]. This control aims to realize an haptic feedback, computing the pressure of the active seat bladders starting from the acceleration signals.
In section 2.3 instead, the pressure model, developed in [9] and in [10], is introduced to describe the lateral pressure between the driver's trunk and the seat. The lateral model and the inflatable bladder model will be used for the model-based pressure cue strategy, proposed in chapter 3.

2.1 The Active Seat system

The active seat is a pneumatic system capable of exerting pressure in specific areas of the driver's body by means of eight inflatable bladders. This system is inspired by the G-seat technology, widely used for static flight simulators. The G-seat is designed to provide the pilot with somatic stimuli, as skin pressure, to reproduce all the forces due to acceleration, braking and fast bends. The general cueing scheme, implemented in the G-seat, is a "surface pressure" philosophy, that requires the seat bladders to inflate or deflate such that the pilot perceived pressure is in the same direction of the aircraft acceleration vector [11].

Similarly, the active seat system is used, in the driving simulators, to provide the driver with the feeling of low frequency accelerations that, due to the limited workspace, can not be recreated with a movement of the platform. The system is usually complemented by an active belts system to transmit to the driver the sensation of braking. It would be impossible to reproduce the sensation of braking just by moving the platform or by activating the bladders of the active seat. In figure 2.1 is shown the active system and its bladders location: bladders

Figure 2.1: Active Seat scheme

2 and 5 provide the pressure to the trunk of driver's body, 1 and 6 to the legs along the lateral direction, 3 and 4 to the back for positive longitudinal acceleration and, finally, 7 and 8 to the glutes along the vertical direction. The bladders are designed to have a distributed contact area and placed to act on the body similarly to what happens in reality. Proportional valves are used to have a progressive and continuous variation of pressure.
In figure 2.2 instead, is shown the active belt system, every belt is activate by a pneumatic muscle.

The typical control strategy, in a static environment, is described in section 2.2: the lateral

Figure 2.2: Active belts scheme

acceleration is used to control the lateral bladders, longitudinal acceleration is used for belt

tension and the bladders in the back, while vertical acceleration is used for the bladders on the bottom.
Conversely, the control strategy is not so straightforward in a dynamic simulator, the active seat system has to adapt real time to the undergoing motion behavior.

Accelerations

For clarity of notation, in the dynamic simulator, the platform accelerations with respect to the world reference frame are denoted as a_x, a_y and a_z. Instead, denoted as $a_{x,drv}$, $a_{y,drv}$ and $a_{z,drv}$ are the accelerations of the driver's center of mass with respect to the seat reference frame. The relation between the two acceleration types is:

$$a_{i,drv} = -a_i$$

for $i \in \{x, y, z\}$, as can be seen in figure 2.3.

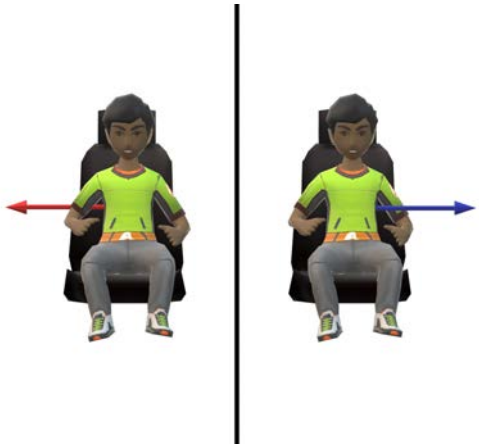

Figure 2.3: Acceleration representation: in red the actual external acceleration of the seat in the World reference frame, in blue the acceleration perceived by the driver with respect to the Seat reference frame (non-inertial frame)

2.2 Haptic feedback

The haptic feedback strategy use the bladders of the active seat to directly transmit information on the vehicle accelerations to the driver. The information is perceived by the driver as a pressure cue in different areas of its body.

The logic behind the active seat computes the pressure inside each air bladder, p_c^{VI}, using the vehicle accelerations and several tunable parameters. The input accelerations are pre-processed to remove the unnecessary high-frequency components and then saturated. By modifying the system parameters, it is possible to tune the feeling depending on the driver, car, and seat. The pressure within the lateral air bladders (number 1-2-5-6 in figure 2.1) is dependent on lateral acceleration; i.e. during a left corner the right lateral cushions are inflated, while left lateral cushions are deflated.

The control scheme is shown in figure 2.4 and as can be seen the pressure induced by the

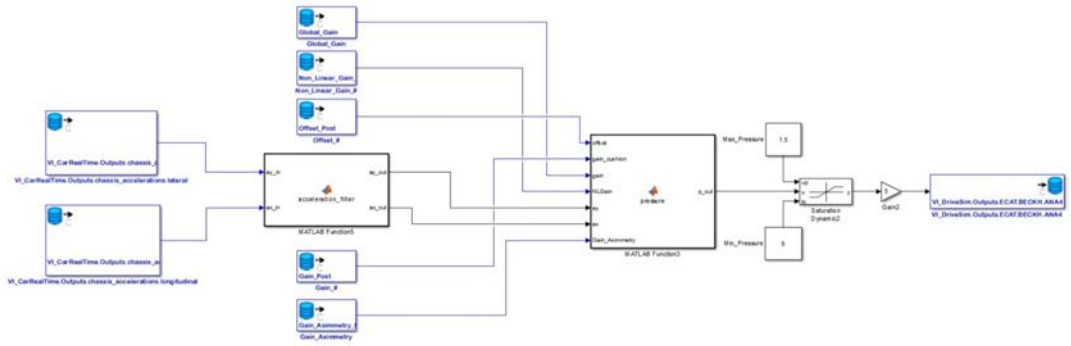

Figure 2.4: Actual control scheme of the Active Seat system

platform movement is not taken into account.

2.3 Pressure model of the driver for the model-based pressure cue

In this section, a model is developed to describe the driver's dynamic and the consequent pressure between its body and the seat.

Only the lateral pressure is taken into account, the longitudinal pressure can be described through a linear version of the lateral model. The vertical model has been neglected since, on driving simulators, vertical forces are not so remarkable.

The model in the following is focused on the pressure exerted between the driver's trunk and the lateral sides of the seat. Following the same principle and tuning the model parameters, the lateral model for the driver's legs can be obtained. The model can be applied both in a real car scenario and in a dynamic driving simulator. The De Wit dynamic model is introduced to consider the friction between the driver and the seat.

The original model development can be found in [9] and [10].

2.3.1 Lateral driver's trunk dynamic

During a vehicle turn, the driver's trunk is pushed toward the side of the seat. To describe the contact pressure, a non-linear model has been developed. Starting from the lateral driver acceleration, the car/platform longitudinal acceleration and the car/platform roll, the model computes, as output, the pressure the driver is subjected to. The lateral dynamic of the body is characterized by means of a mass-spring-damper model, represented by the following equation:

$$m\ddot{d}_y + C(d_y)\dot{d}_y + K(d_y)d_y = ma_{y,drv} \tag{2.1}$$

where d_y, $\dot{d}_y$ and $\ddot{d}_y$ are respectively the position, velocity and acceleration of the center of mass of the driver's trunk along the lateral direction. The value of m is the driver's mass subjected to lateral acceleration. The coefficients $K(d_y)$ and $C(d_y)$ are respectively the stiffness and damping coefficients, modeling both the seat reactions and the driver's intrinsic free-body properties. The term $F = ma_{y,drv}$ is the external force applied on the driver's center of mass.

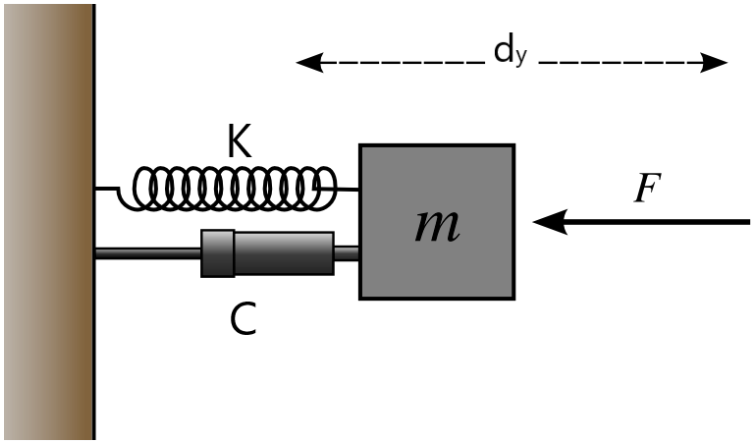

Figure 2.5: Mass spring damper model

Therefore equation 2.1 consider:

- $F = ma_y$ the external force that acts on the center of mass of the driver
- $F_v = c(d_y)\dot{d}_y$ the damping force opposed to the lateral movement of the driver
- $F_k = k(d_y)d_y$ the spring force opposed to the lateral movement of the driver

First of all, the driver's trunk inertial mass m has to be estimated. The total mass of the driver has been assumed to be $75kg$. In [12], several studies have presented formulae that estimate

the mass and the location of the center of mass of the various segments based on cadaver studies. Using Plagenhoef's data, it has been found that the whole trunk with arms and hands constitutes about 67% of total body weight for a male, thus $M \approx 50kg$. Moreover, the center of mass location of the human trunk is about 50% of the length of the trunk itself. To take into account the driver's body inertial properties, the trunk cannot be considered as a point mass, but we model it as a homogeneous rod of length L and mass M, rotating about one end. The inertia is then:

$$I = \frac{1}{12}ML^2 + M\left(\frac{L}{2}\right)^2 = \frac{1}{3}ML^2. \tag{2.2}$$

Defining h as the distance between the center of mass of the driver's trunk and the point of rotation, the trunk angle can be connected to the lateral displacement by $h\sin(\beta) = d_y$. For small values of the angle β the sine can be approximated with the angle itself. Deriving the previous relation two times with respect to time, we have an approximation of the angular acceleration: $\ddot{\beta} = {\ddot{d}_y}/{h}$. By the definition of angular momentum as:

$$\bar{M}_{ang} = \bar{F}\bar{h}, \tag{2.3}$$

where $\bar{F}$ is the external force vector and $\bar{h}$ is the position vector of the application point, we can express the angular momentum magnitude as the force multiplied by the arm. Finally, according to the principle of angular momentum conservation we obtain:

$$Fh = I\ddot{\beta}$$

and thus

$$F = \frac{1}{3}M\left(\frac{L}{h}\right)^2 \ddot{d}_y$$

Hence, assuming the human trunk as homogeneously distributed, the arm of the applied forces is $h = {L}/{2}$ that leads to:

$$F = \frac{4}{3}M\ddot{d}_y = m\ddot{d}_y.$$

To consider the inertial properties of human body, the inertial mass to be considered in the trunk dynamic is $m = \frac{4}{3}M$ and thus, recalling that the trunk mass is assumed to be $M = 50kg, m = 67kg$.

The model of the seat embedded in the lateral model consists of a combination of a non-linear spring and a non-linear damper to mimic the seat reaction on the driver's dynamic. The spring term defines the low-frequency force reaction of the seat, limiting the driver's trunk movement. Instead, the damping term models the impact reaction due to the collision between the driver and the side of the seat limiting the driver's velocity. Both terms have low values around the seat zero position and grows rapidly as the displacement d_y grows. To represent this trend, a polynomial has been chosen, in particular a quadratic one. Then, we can write:

$$k_{seat}(d_y) = k_2 d_y^2$$
$$c_{seat}(d_y) = c_2 d_y^2$$

where k_{seat} and c_{seat} are constant parameters depending on the seat geometry and materials. Moreover, the human body has an intrinsic stiffness that holds the mass to fall laterally, and an intrinsic damping behavior when subjected to an external force. In the model, we consider these contributions through the free-body parameters k_0 for stiffness and c_0 for damping. Then, the overall model parameters are:

$$K(d_y) = k_2 d_y^2 + k_0 \tag{2.4}$$
$$C(d_y) = c_2 d_y^2 + c_0 \tag{2.5}$$

and their characteristics can be seen in figure 2.6.

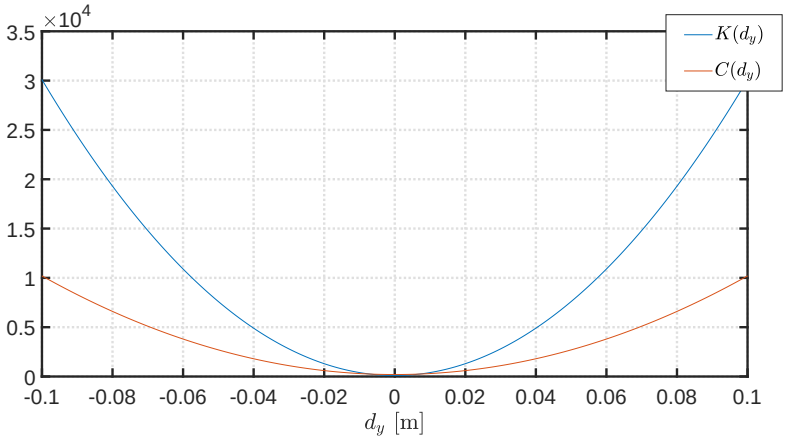

Figure 2.6: Stiffness and damping characteristics

2.3.2 Friction component and longitudinal coupling

To improve the realism of the model, the frictions between the human body and the seat pan/backrest has been considered. The classical models, for example, Coulomb and viscous friction can lead to performance problems for low-velocity tracking or numerical problems in case of zero-crossing velocity. The dynamic model proposed by De Wit et al. in [13] is considered because all the important phenomena that occur between the two contact surfaces are taken into account. In particular, De Wit's model shows good description capabilities for hysteretic behaviors and variations in the break-away force. Complex models are mostly

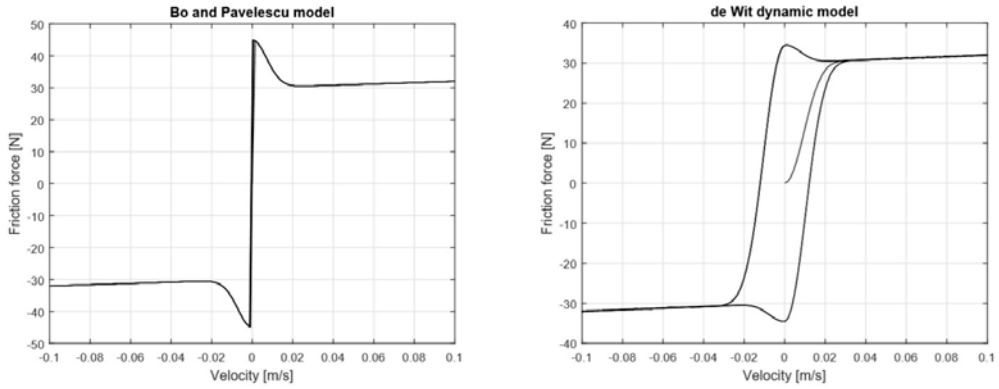

(a) Bo and Pavelescu static model. (b) de Wit et al. dynamic model.

Figure 2.7: Behavior comparison at zero crossing velocity for static and dynamic friction models

built upon the simple model elements with additional features, which can handle dynamic behavior. In figure 2.7, a comparison between a static model and De Wit model at zero crossing velocity.

When two rigid bodies get in touch, the irregular surfaces make contact through microscopic asperities. In presence of a tangential force, the bristles deflect causing a friction force between the two objects. If the tangential force is sufficiently large and the bristle deflection is enough, the two objects will slip. De Wit model is based on the average behavior of the bristles, which is denoted by z and modeled by:

$$\frac{dz}{dz} = v - \frac{|v|}{h(v)}z, \tag{2.6}$$

where $v = \dot{d}_y$ is the relative velocity between the two objects. The function $h(v)$ is positive and depends on many factors such as material properties, lubrication and temperature. The

$h(v)$ function chosen to characterize the Stribeck effect is:

$$h(v) = F_d + (F_s - F_d)\, e^{(v/v_s)^2} \tag{2.7}$$

where N is the reaction force perpendicular to the seat surface, $F_d = \mu_d N$ and $F_s = \mu_s N$ are respectively the dynamic and static friction forces and v_s is the Stribeck velocity. The friction parameters μ_s and μ_d depends on the seat material and drivers' clothes. The friction force generated bending the bristles can be computed exploiting the relation:

$$F_{fric} = \sigma_0 z + \sigma_1 \frac{dz}{dt} \tag{2.8}$$

The dynamic friction force is hence characterized by the two parameters σ_0, σ_1 and the function $h(v)$.
An important aspect to notice is that the friction depends on the normal force N, coupling the lateral model with the longitudinal one: the higher the external longitudinal acceleration, the more the human body is pressed against the seat, increasing the normal reaction. Conversely, in case of a longitudinal deceleration, the driver's trunk is moved away from the seat backrest reducing the normal reaction up to zero when the detachment between the two bodies occur. The seat is supposed to have an inclined backrest of an angle α with respect to the vertical axis. The normal force N is then:

$$N = m a_x \cos(\alpha) + M g \sin(\alpha) \tag{2.9}$$

where a_x is the external longitudinal acceleration and M is the driver's trunk mass on the seat pan.

To avoid numerical problems, in the implementation of the De Wit model F_s and F_d are defined as nominal values of the static and dynamic friction respectively. The instantaneous values $\bar{F}_s$ and $\bar{F}_d$ of these friction values are computed by means of the function:

$$g_N(N) = \frac{1}{\pi} \arctan(N) + 0.55. \tag{2.10}$$

The function $g_N(N)$, shown in 2.8, modulates the nominal friction values with respect to the actual normal reaction N between the driver and the backrest of the seat.

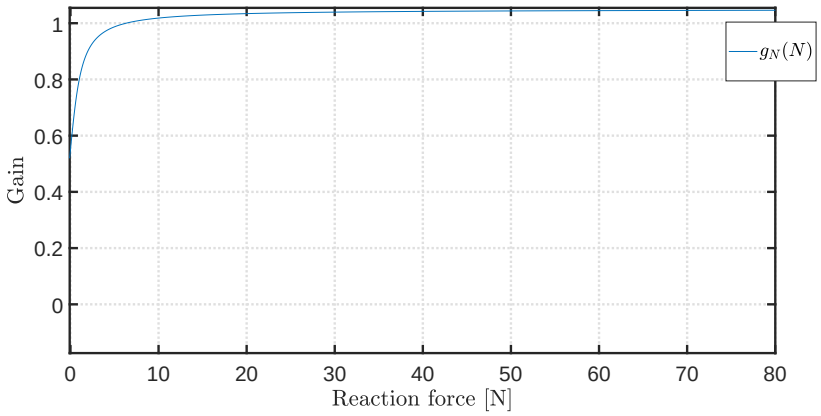

Figure 2.8: Nominal friction modulation function

As can be seen in figure 2.9, the friction computation leads to an overestimated friction force, almost preventing the driver's body to move. To overcome this problem, we introduce a correction gain of the nominal friction values, such as:

$$F'_s = K_{fric} F_s \tag{2.11}$$

$$F'_d = K_{fric} F_d \tag{2.12}$$

The gain $K_{fric} = 0.1$ has been chosen by inspection on the driver's lateral dynamic, as shown in figure 2.9. The computed parameters F'_s and F'_d will be used instead of F_s and F_d in the function $h(v)$.

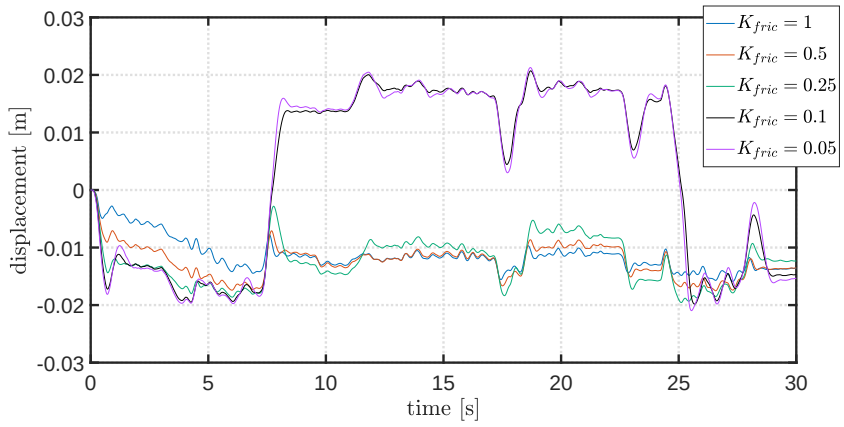

Figure 2.9: Driver's lateral displacement on the simulator for different values of the correction gain K_{fric}

2.3.3 Lateral tilt coordination

An additional component with an important role in the lateral model is the tilt coordination. The seat inclination has a major role in the driver's perception, in particular in a dynamic simulator. Due to a reduced workspace for the platform motion, a simple tangential translation is not sufficient to ensure the reproduction of a real vehicle acceleration.

The vestibular system is the sensory apparatus that provides the leading contribution to the sense of balance and spatial orientation in the human being. Its main function is to control motion and equilibrium by providing information about the transactional and rotational accelerations that are acting on the body, including the effect of gravity force. It is located in the inner ear and composed by two subsystems:

- the semicircular canals, which are responsible for the perception of the rotations the body is subject to;
- the otolithic organs, which provide linear motion sensation in human beings for specific force, meaning the combination of transactional acceleration and gravity force.

The human being is incapable to distinguish between translational and gravitational accelerations through otoliths only. The motion cueing algorithms exploit this phenomenon to cheat the driver's sensory system to perceive a greater lateral acceleration by tilting the platform with an appropriate angle ϕ. The consequences of this strategy in the lateral model, both in the dynamic simulator and in the real car scenario, is a new force term added to the external force acting on the driver:

$$F_{tilt,y} = -mg\sin(\phi) \tag{2.13}$$

where the −sign is used only to have the right direction of the component in the seat reference frame. Using the small angle linearization we obtain:

$$F_{tilt,y} = -mg\phi \tag{2.14}$$

that is the tilt coordination term that will be added to the right term of equation 2.1 to take into account the roll dynamic of the system in the lateral model.

2.3.4 Lateral model and lateral pressure computation

To sum up all the previous considerations on friction and tilt coordination on the lateral dynamic of the trunk's driver, we can rewrite equation 2.1 as:

$$m\ddot{d}_y + C(d_y)\dot{d}_y + K(d_y)d_y = ma_{y,drv} + F_{tilt,y} - F_{fric} \tag{2.15}$$

where F_{fric} and $F_{tilt,y}$ are the forces computed respectively in 2.8 and 2.14. For convenience, the model can also be expressed as a system of first-order differential equations such as:

$$\begin{cases} \ddot{d}_y &= a_{y,drv} - \frac{K(d_y)d_y}{m} - \frac{C(d_y)\dot{d}_y}{m} - \frac{F_{fric}}{m} + \frac{F_{tilt,y}}{m} \\ \dot{z} &= \dot{d}_y - \frac{|d_y|}{h(d_y)}\dot{d}_y \end{cases} \tag{2.16}$$

where:

$$\begin{aligned} F_{fric} &= \sigma_0 z + \sigma_1 \frac{dz}{dt} \\ F_{tilt,y} &= -mg\sin(\phi) \\ h(\dot{d}_y) &= F_d + (F_s - F_d)\, e^{\left(\dot{d}_y/v_s\right)^2} \\ F_s &= \mu_s N \\ F_d &= \mu_d N \\ N &= ma_x \cos(\alpha) + Mg\sin(\alpha) \end{aligned}$$

The model receives in input the lateral driver acceleration $a_{y,drv}$, the car/platform longitudinal acceleration a_x and the car/platform roll angle ϕ and computes the driver's trunk lateral dynamic d_y, $\dot{d}_y$ and $\ddot{d}_y$.

As stated at the start of this chapter, the desired output of the model is the lateral contact pressure on the driver. Exploiting the definition of pressure as the ratio between the applied force and the area of application, the lateral trunk pressure can be computed starting from the seat reaction force and the contact area between seat and the driver. Then, we can write:

$$p_{lat} = \frac{\left(K(d_y) - k_0\right) d_y + \left(C(d_y) - c_0\right) \dot{d}_y}{A} \tag{2.17}$$

where A is the contact area.

2.4 The inflatable bladder model or the model-based pressure cue

In [9] is presented a model to describe the inner bladder pressure of an active seat bladder starting from a desired contact pressure on the driver's trunk and its displacement on the seat. The contact can be developed as a static mechanical contact without friction. In the following sections, we start from a simplified case study, then we further develop the bladder-trunk contact mechanic.

2.4.1 Contact mechanics

First, we consider a simplified example of the contact mechanics between a rigid sphere and an elastic half-space. From [14], considering an Hertzian pressure distribution $p(r)$ on a circular plane area of radius a we can write:

$$p(r) = p_0 \left(1 - \frac{r^2}{a^2}\right)^2 \tag{2.18}$$

with $r = \sqrt{x^2 + y^2}$ distance between the considered point and the origin of the contact pressure and p_0 pressure on the normal axis on the origin. The pressure applied on the elastic object lead to a vertical deformation of the object itself. The points of the elastic half-space are moved from their original position of:

$$u_z = \frac{p_0}{4E^* a}\left(2a^2 - r^2\right) \qquad r < a \tag{2.19}$$

where the parameter E^* describes the elastic characteristic of the contact. The parameter E^* is connected to the Young's modulus, defining the relationship between stress (force per unit area) and strain (proportional deformation) in a material in the linear elasticity regime of a uni-axial deformation, by the equation:

$$E^* = \frac{E}{(1 - \nu^2)}. \tag{2.20}$$

In the previous equation, ν is the Poisson's ratio defined as the negative of the ratio of (signed) transverse strain to (signed) axial strain. For small values of these changes, ν is the amount of transversal expansion divided by the amount of axial compression. Both parameters E and ν depends only on the material of the considered object. During a vertical mechanical contact between the rigid sphere and the elastic half-space without friction, the vertical displacement

can be geometrically computed as::

$$u_z = d - \frac{r^2}{2R} \tag{2.21}$$

where R is the sphere radius and d the compenetration of the two objects on the normal axis of the contact point. From the equivalence of equations 2.19 and 2.21, we can obtain a relationship to compute the contact pressure starting from the compenetration d of the two objects and the elastic properties:

$$p_0 = \frac{2E^*}{\pi}\sqrt{\frac{d}{R}} \tag{2.22}$$

2.4.2 Bladder-trunk contact mechanics

Considering the bladder-trunk mechanics there are some key differences with respect to the case study of the previous section:

- the contact area is not circular
- both the bladder and the driver's trunk are elastic bodies
- elastic properties of the objects and the bladder radius depend on the inner bladder pression
- the compenetration between trunk and bladder depends on the trunk instantaneous displacement on the seat and the inner bladder pression

Contact area

The contact area, represented in figure2.10, between the driver's trunk and the active seat bladder can be assumed as approximately elliptical, with axes a and b. We can approximate the bladder as a sphere with radius:

$$\tilde{R} = \sqrt{R_a R_b} \tag{2.23}$$

the geometric mean of the curvature radii on the ellipse axes.

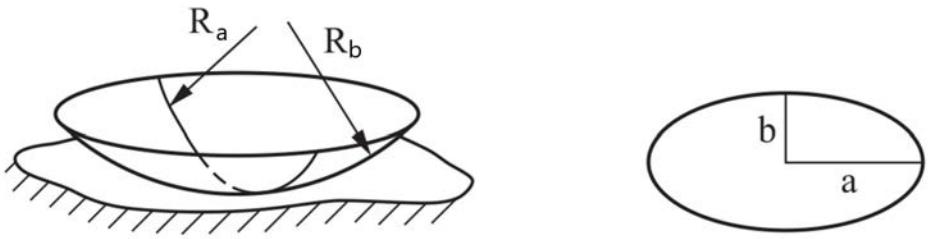

Figure 2.10: Elliptical contact area

Bladder radius and inner pressure relation

In [15], Muller propose a mathematical formula to describe the connection between the radius of an inflatable balloon of radius R_{ball} and its inner pressure p_{ball}, as:

$$p_{ball}(R_{ball}) = 2s_1 \frac{d_0}{r_{ball,0}} \left(\frac{r_{ball,0}}{R_{ball}} - \left(\frac{r_{ball,0}}{R} \right)^7 \right) \left(1 - \frac{s_1}{s_{-1}} \left(\frac{r_{ball,0}}{R} \right)^2 \right) \tag{2.24}$$

where d_0 and r_0 are the thickness and the radius of the balloon, respectively, before inflation, and s_1 and s_{-1} are the two constants of a Mooney–Rivlin material. In figure 2.11 is shown the trend of $p_{ball}(R_{ball})$ and, as can be seen, it is a non-monotonic function.

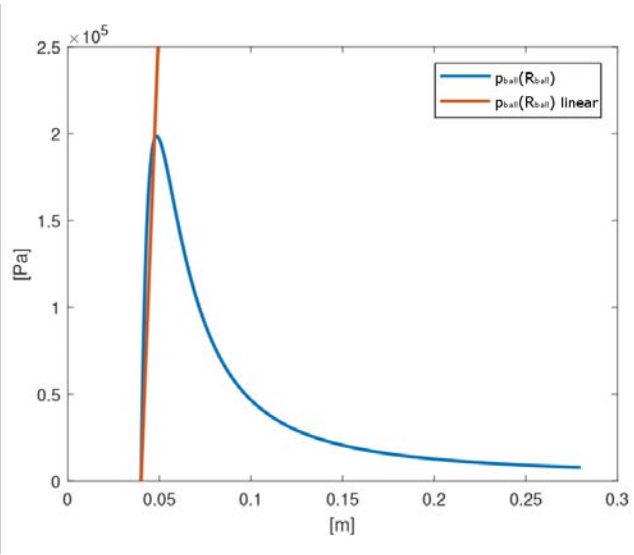

Figure 2.11: Non-monotonic relation between balloon inner pressure p_{ball} and balloon radius

Equation 2.24 can be linearized under the following hypothesis:

- In the contact area approximation, radii R_a and R_b are uniformly varying with the varying of the inner pressure
- $r_0 \neq 0$, the bladder radius is different from zero before inflation
- The bladder radius can be expressed as $\tilde{R} = \Delta\tilde{R} + r_0$
- $\Delta\tilde{R} < 1.5cm$

obtaining the following equation:

$$p_c = K_{bl}\Delta\tilde{R} \tag{2.25}$$

with K_{bl} suitable constant conversion gain and p_c inner bladder pressure.

Elastic properties of the bladder-trunk contact

In the case of the driver's trunk and active seat bladder contact, both objects have elastic properties. The following relationship holds in this situation:

$$\frac{1}{E^*} = \frac{1-\nu_{drv}}{E_{drv}} + \frac{1-\nu_{bl}(p_c)}{E_{bl}(p_c)} \tag{2.26}$$

where the subscript *drv* identifies the constant driver's parameters while *bl* identifies the bladder parameters dependant on the inner pressure.
The overall elastic contact characteristic of the system shows a dependency on the inner pressure state of the bladder, the relation can be expressed starting from the linearized equation in 2.25 as:

$$E^* = Gp_c = G\left(K_{bl}\Delta\tilde{R}\right) = G_{bl}\Delta\tilde{R} \tag{2.27}$$

where G, K_{bl} and $G_{bl} = GK_{bl}$ are constant conversion gains.

Compenetration and bladder-trunk dynamic

During a driving simulation, the compenetration between the driver's trunk and the active seat bladder can change:

- The driver' trunk displacement changes due to the external forces

- The inner bladder pressure changes, and as consequence also the bladder radius changes
- Both driver's trunk displacement and bladder radius change

Under the assumption of always contact between the driver's trunk and the bladder we can define the compenetration of an opposed pair of bladders along a movement direction as:

$$\epsilon_a = \begin{cases} x & x > 0 \\ 0 & \text{otherwise} \end{cases} \tag{2.28}$$

$$\epsilon_b = \begin{cases} -x & x < 0 \\ 0 & \text{otherwise} \end{cases} \tag{2.29}$$

where x is the driver's trunk displacement along the movement direction. The subscript a identifies the bladder placed in the positive part of the movement axis, the subscript b instead identifies the bladder placed in the negative part of the movement axis. The depth of the compenetration can be computed for a generic bladder i as:

$$d_i = \Delta\tilde{R} + \epsilon_i \tag{2.30}$$

Inner bladder pressure computation

For the lateral model, in a dynamic driving simulator, the overall pressure $y_{p,lat}$ on the driver's trunk is the sum of the pressure induced by platform movement p_{lat} (shown in 2.17) and the contact pressure between the driver's trunk and the active seat bladders p_0, is:

$$y_{p,lat} = p_{lat} + p_0. \tag{2.31}$$

We can express the contact pressure as function of the bladder radius variation. Substituting equations 2.25 and 2.30 in 2.22 and expressing the bladder radius $\tilde{R}$ as function of $\Delta\tilde{R}$, we get for a generic bladder i:

$$p_{0,i} = \frac{2G_{bl}\Delta\tilde{R}}{\pi}\sqrt{\frac{\Delta\tilde{R} + \epsilon_i}{\Delta\tilde{R} + r_0}} \tag{2.32}$$

Inverting the relation in equation 2.32 we can express the bladder radius variation in function of the desired contact pressure on the driver:

$$\Delta\tilde{R} = \frac{\frac{p_{0,i}^2\pi^2}{4G_{bl}^2\Delta\tilde{R}^2}r_0 - \epsilon_i}{1 - \frac{p_{0,i}^2\pi^2}{4G_{bl}\Delta\tilde{R}^2}} \tag{2.33}$$

that can be expressed ad a third order equation in the unknown $\Delta\tilde{R}$:

$$4G_{bl}^2\Delta\tilde{R}^3 + 4G_{bl}^2\epsilon_i\Delta\tilde{R}^2 - \pi^2 p_{0,i}^2\Delta\tilde{R} - p_{0,i}^2\pi^2 r_0 = 0 \tag{2.34}$$

Since, $\Delta\tilde{R}$, ϵ_i and $p_{0,i}$ are always positive quantities, equation 2.34 is a real coefficient equation with only one change of sign and for the Descartes rule equation 2.34 has at most one positive root δ. Moreover, since the solution of the discriminant equation of 2.34 leads to at least one positive root, we can assert that δ is also the unique positive solution.
Finally, exploiting equation 2.25 we can compute the inner bladder pressure to exert on the driver's trunk a desired contact pressure with a generic bladder i:

$$p_c = K_{bl}\delta \tag{2.35}$$

In the real physical system, the signal p_c is the inner pressure of the bladders that will be converted in the voltage control signal of the the electro-pneumatic valves by a re-scaling operation .

3

Enhanced model-based pressure cue and control system design

In this chapter, the model-based pressure cue approach is presented. The goal of this approach is to reproduce the real car driving experience, mimicking the pressure cues the driver perceives in the real car. This strategy employs a nonlinear model to take into account the driver's movement in the computation of the control signals. The lateral pressure model, described in the section 2.3, is further developed to achieve a better characterization of the driver's lateral dynamic.
In section 3.2, the feedforward control strategy is presented. The computed control signals take into account the pressure induced by the platform movement.
At the end of the chapter, a different control scheme is proposed, exploiting an MPC strategy, to track a somatosensory reference signal and to compensate for the active seat actuators delay.

3.1 Further lateral model development

The lateral model presented in the previous chapter computes the lateral pressure on the driver's trunk due to the car or platform movement. The model receives, in input, the lateral driver acceleration, the car or platform longitudinal acceleration and the car or platform roll. The model is written, as system of first order differential equations, in 2.16.

3.1.1 Lateral model damping hysteresis

As discussed in section 2.3.1, the seat behavior is modeled by two forces:

$$F_{stiff} = k_{seat}(d_y)d_y \qquad \text{where} \qquad k_{seat}(d_y) = k_2 d_y^2 \tag{3.1}$$

$$F_{damp} = c_{seat}(d_y)\dot{d}_y \qquad \text{where} \qquad c_{seat}(d_y) = c_2 d_y^2 \tag{3.2}$$

the sum of which is the seat reaction force due to the contact with the driver. These two forces limits the lateral driver's trunk dynamic mimicking the sides of the seat: as example, in the entering section of a turn, the driver's trunk is moved toward the side of the seat. The reaction force limits the driver movement, and allows to compute the contact pressure through equation 2.17.
In the exiting phase of a turn instead, the driver's trunk moves toward the center of the seat decreasing the contact pressure with the side. During this transition, since the driver's trunk is moving in the opposite direction with respect to the contact point, the seat has no damping effect on the driver's dynamic.
In general, the seat has a damping component when the driver is moving toward a side of the seat, instead, when the driver is moving toward the center, there are no damping effects. In model 2.16, the seat damping force is considered in both directions, leading to an error in the computed contact pressure when the driver is moving from the side to the center. The desired behavior can be described by means of an hysteresis function, since the damping behavior of the seat depends on the system state and its history: the damping of the seat grows as the displacement grows, when the driver displacement and velocity have the same sign, instead the damping is zero when driver displacement and velocity are of opposite sign. The damping coefficient for the lateral model can be write as:

$$c_{seat}^{hyst}(d_y, \dot{d}_y) = \begin{cases} c_2 d_y^2 & d_y \dot{d}_y > 0 \\ 0 & otherwise \end{cases} \tag{3.3}$$

In figure 3.1 a comparison between the computed contact pressure with $c_{seat}(d_y)$ and $c_{seat}^{hyst}(d_y, \dot{d}_y)$ in the seat model.

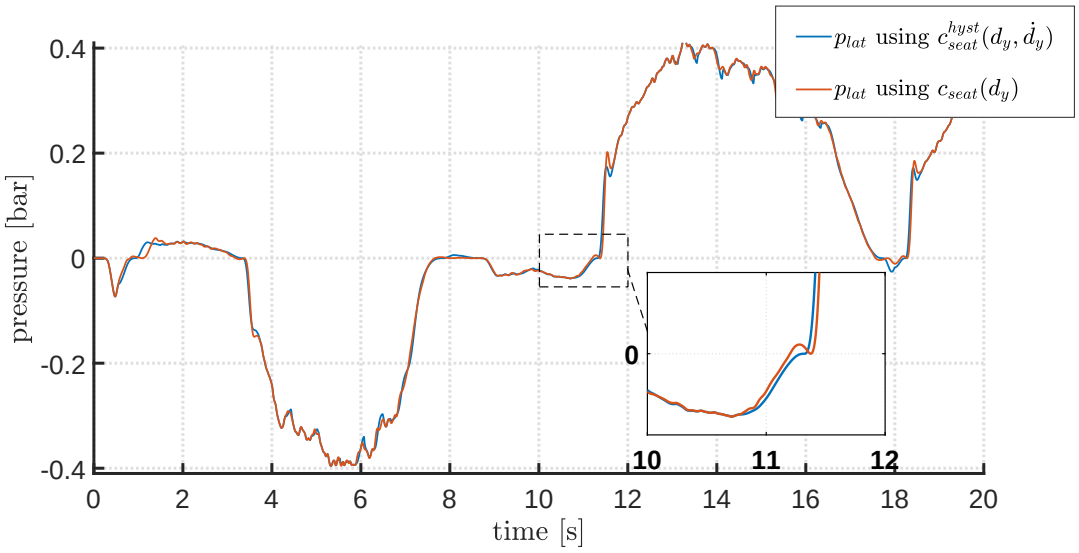

Figure 3.1: Comparison between the computed contact pressure with $c_{seat}(d_y)$ and $c^{hyst}_{seat}(d_y, \dot{d}_y)$

3.1.2 The lateral gravity component

The driver's trunk is modeled as an inverse pendulum with an homogeneous rod of length L and mass M. The sum of the forces acting on the driver's center of mass comports both a lateral displacement and and inclination. Because of this driver's trunk inclination, the projections of the gravity force on the Y and Z axes of the seat are different from zero. In particular, the projection component on Y axis contributes both to the lateral driver's dynamic and the contact pressure with the seat: the weight applied on side of the seat modify the seat reaction force and, as consequence, the contact pressure.

As can be seen in the free body diagram in figure 3.2, the gravity component term for the lateral model can be computed starting from d_y and $h = {}^{L}/_{2}$, height of the driver's center of mass:

$$h' = \sqrt{d_y^2 - h^2} \tag{3.4}$$

$$\beta(d_y) = \arctan({}^{d_y}/_{h'}) \tag{3.5}$$

$$F'_{grav} = Mg\sin(\beta(d_y)). \tag{3.6}$$

The F'_{grav} is the gravity component acting perpendicularly to the driver's trunk. The gravity component contributing in the lateral dynamic is the projection of F'_{grav} on the seat Y axis:

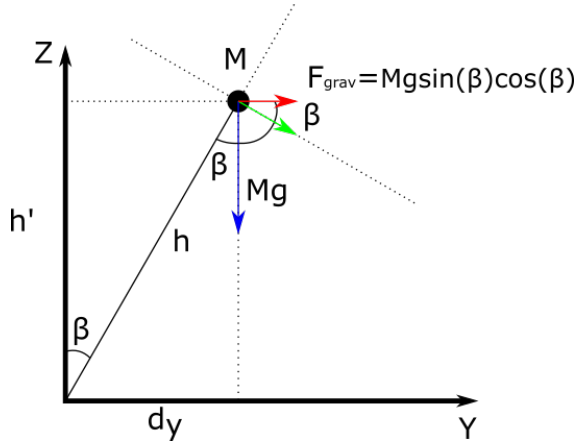

Figure 3.2: Free body diagram of the system. In blue the gravitational force, in green its perpendicular projection with respect to the trunk, and in red the gravitational force component acting in the lateral model.

$$F_{grav} = Mg \sin(\beta(d_y)) \cos(\beta(d_y)). \tag{3.7}$$

The implemented model for the gravity component presents also some limitations. In the human being the lateral inclination of the shoulders with respect to the driver's hips is limited by the spinal column, composed by 33 vertebrae. The vertebrae are separated by disks made of cartilage, which act as cushions. The lateral inclination of the spinal column is hence influenced by the relative angle constraints between every vertebra and the next one. A proper model of the spinal column would be a series of 33 inverse penduli, with all the relative angle constraints. Fixing the driver's hips on the seat and progressively inclining laterally the shoulders leads the spinal column to assume an arc-like form. The implemented driver's trunk model instead, is composed by a single inverse pendulum. For the same angular displacement of the shoulders, the arc-like figure assumed by the spinal column in the 33 inverse penduli model, leads to a lower angular displacement of the center of mass of the driver's trunk than in the single inverse pendulum model. A representation of this fact is shown in figure 3.3. The overestimated angle β, lateral angular displacement of the center of mass, comports an overestimated component of the gravity force acting on the driver's lateral trunk dynamic. The angle β is multiplied by a correction gain before computing the projection of the gravity force to overcome this problem, obtaining β':

$$\beta'(d_y) = K_{grav} \arctan(^{d_y}/_{h'}) \tag{3.8}$$

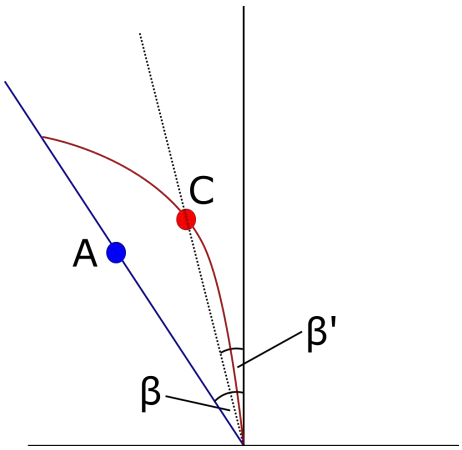

Figure 3.3: Comparison between the center of mass angular displacements. The point **A** is the center of mass of the driver's trunk if modeled by one rigid inverse pendulum, instead **B** is the center of mass of the driver's trunk if modeled with 33 inverse penduli.

In figure 3.4, the lateral displacement of the driver's trunk is shown for different values of K_{grav}. The chosen value is $K_{grav} = 0.03$ by inspection on the model dynamic.

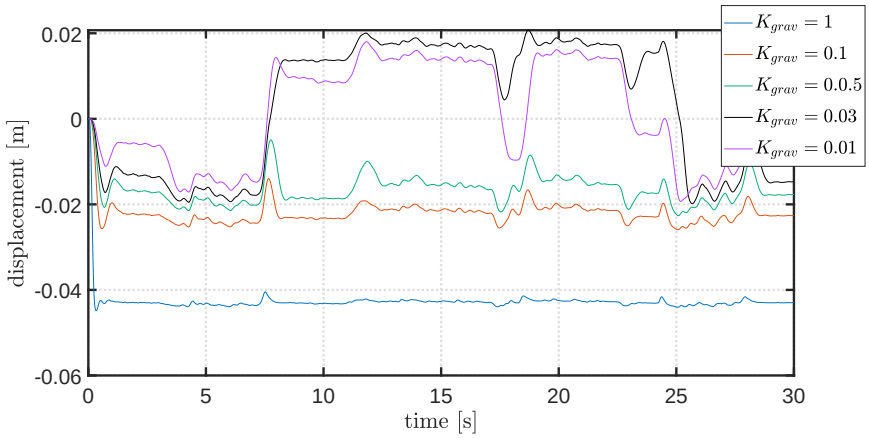

Figure 3.4: Comparison between different values of the correction term for the gravitational component

In figure 3.5 is shown the comparison of the driver's lateral displacement with and without considering F_{grav}.

The pressure is computed as seat normal reaction force over the area of contact, hence to

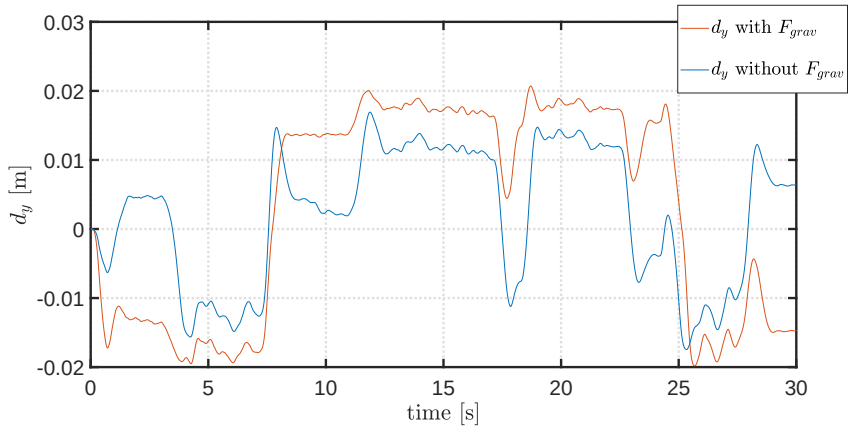

Figure 3.5: Comparison between the lateral driver displacement with and without the gravitational component

account for the new contribution we can express the contact pressure as:

$$p'_{lat} = \frac{(K(d_y) - k_0)\, d_y + (C(d_y) - c_0)\, \dot{d}_y}{A} + \frac{F_{grav}}{A} \tag{3.9}$$

3.1.3 The expanded lateral model

To include all the previous considerations on the seat damping factor and the gravity component we can rewrite model 2.16 as:

$$\begin{cases} \ddot{d}_y &= a_{y,drv} - \frac{K(d_y)d_y}{m} - \frac{C(d_y)\dot{d}_y}{m} - \frac{F_{fric}}{m} + \frac{F_{tilt,y}}{m} + \frac{F_{grav}}{m} \\ \dot{z} &= \dot{d}_y - \frac{|d_y|}{h(d_y)}\dot{d}_y \end{cases} \tag{3.10}$$

where:

$$K(d_y) = k_2 d_y^2 + k_0$$
$$C(d_y, \dot{d}_y) = c_{seat}^{hyst}(d_y, \dot{d}_y) + c_0$$
$$F_{fric} = \sigma_0 z + \sigma_1 {}^{dz}/_{dt}$$
$$F_{tilt,y} = -mg\sin(\phi)$$
$$F_{grav} = Mg\sin(\beta(d_y))\cos(\beta(d_y))$$
$$h(\dot{d}_y) = F_d + (F_s - F_d)\, e^{\left(\dot{d}_y/v_s\right)^2}$$
$$F_s = \mu_s N$$
$$F_d = \mu_d N$$
$$N = ma_x\cos(\alpha) + Mg\sin(\alpha)$$

The contact pressure is then computed from the driver's trunk dynamic by means of equation 3.9.

3.2 Feedforward control

The feedforward control developed in this section is based on the pressure model 3.10. We first consider the lateral bladders control, specifically bladders 2 and 5 in figure 2.1. The control strategy aims to reproduce the driver's contact pressure of a real car scenario in the simulator platform. To achieve this objective, the control scheme of figure 3.6 has been implemented. For easiness of notation, from now on, the label *chassis* will be used to denote the

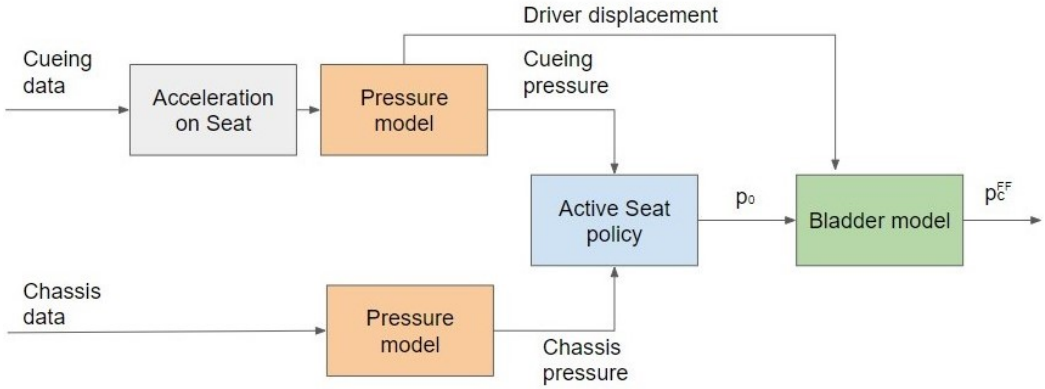

Figure 3.6: Feedforward pressure control scheme

quantities connected to the real car scenario, conversely, the label *cueing* will denote the quantities tied to the simulator platform.
First, we consider the real car data. Applying the lateral model 3.10, the lateral contact pressure is computed for a driver in a real car. In the same way, starting from the simulator data, the lateral driver's contact pressure, induced by the platform movement, is computed. To reproduce in the dynamic simulator the same pressure of the real car, the active seat bladders contribution must be derived. The desired outcome, for any given time, is that:

$$y_{p,lat}^{chassis} = y_{p,lat}^{cueing} = p'_{lat} + p_{0,lat} \tag{3.11}$$

where $y_{p,lat}$ is the overall trunk pressure, p'_{lat} is the pressure induced by the platform movement, and $p_{0,lat}$ is the lateral bladder contribution. The computation of the desired contact pressure for the active seat bladders can be achieved through various strategies, an in-depth discussion is presented in the next subsection. Once that $p_{0,lat}$ is obtained, knowing the driver's trunk dynamic and exploiting the inflatable bladder model shown in section 2.4, the control signals for the active seat valves can be computed.

3.2.1 The Active Seat compensation policies

The active seat compensation policies are different strategies for the computation of the contact pressure p_0 of the bladders. The simulator platform aims to reproduce the driver's perceived accelerations of the real car and the more limited is the simulator workspace, the more the pressure induced by the platform movement differs from the pressure in the real car. The major differences between the two pressure signals are:

- the driver pressure on the simulator anticipating the real car one
- the driver pressure on the simulator delayed with respect to the real car one
- the pressure on the simulator and in the real car are perceived by the driver on different sides, i.e. in the real car the acceleration magnitude pushes the driver's body on the opposite side of the seat, whereas in the simulator it is not intense enough to do so.

When one of these situations occurs, the computation of p_0 is not straightforward and the active seat policies tackle the problem defining different behaviors for different cases.

Straight

The *Straight* policy of the active seat is the simpler one considered. This strategy consists of the direct difference between the two input signals $p_{chassis}$ and p_{cueing}. This strategy can easily be written as:

$$p_0 = p_{chassis} - p_{cueing}. \tag{3.12}$$

In this case, the possible inconsistencies are not handled.

Consistency conditions

The *Consistency conditions* policy is developed to identify the inconsistencies between the input signals $p_{chassis}$ and p_{cueing} and compute accordingly the contact pressure of the bladders p_0. The first condition checked is if the two input signals computes pressures on the same side of the driver. If this condition is not passed, the active seat can not satisfy the desired relation 3.11. Similarly, in the case that the instantaneous pressure induced by the simulator is higher than the computed pressure on the real car, no action of the active seat can lead to satisfy the desired outcome 3.11.
Moreover, in this strategy, the perceived acceleration $a^{chassis}_{drv,vest}$ is taken into account and obtained from the real car acceleration by means of a vestibular filter. The filter is the one shown in [10], and derived from the previous works [16] and [17], adopting the mathematical model proposed in [18] by Telban and Cardullo. The vestibular transfer function for tangential accelerations is then:

$$W(s) = \frac{\hat{f}(s)}{f(s)} = 0.4\frac{1+10s}{(1+5s)(1+0.016s)} \tag{3.13}$$

where $\hat{f}(s)$ is the perceived transitional force along the considered axis, whereas $f(s)$ is the real force. This strategy uses as last consistency check if the perceived acceleration on the real car is directed toward the same side of the seat in which the pressure is computed in. The overall strategy can be written as:

$$if \begin{cases} sign(p_{chassis}) = sign(p_{cueing}) \\ |p_{chassis}| \geq |p_{cueing}| \\ sign(p_{chassis}) = sign(a^{chassis}_{drv,vest}) \end{cases} \Rightarrow \quad p_0 = p_{chassis} - p_{cueing} \tag{3.14}$$

Otherwise $p_0 = p_{chassis}$.
It is important to notice that, in case of an inconsistency detection, a sort of fallback strategy is adopted: the active seat bladders mimic the real car pressure signal ignoring the pressure induced by the simulator. This policy defines an appropriate behavior when the input data from the pressure models are inconsistent and tries to maximize the real car pressure tracking. However, this strategy introduces also some discontinuities, leading to some artifacts in the control signals of the active seat.

Split&Splice

The *Split&Splice* policy is presented to overcome the inconsistencies of the pressure models and also to prevent discontinuities in the reference contact pressure signal. The idea is to consider every bladder separately and then recreate the contact pressure signal of the opposite pairs of bladders. First, the pressure signals computed, both in the real car scenario and in the simulator, are split into positive and negative parts, denoted p^+ and p^- respectively. The reference contact pressure signal is computed between the two positive signals, and the two negative ones. The strategy can be written as:

$$\begin{cases} p_0^{\pm} = p_{chassis}^{\pm} - p_{cueing}^{\pm} & if \quad |p_{chassis}^{\pm}| \geq |p_{cueing}^{\pm}| \\ p_0^{\pm} = 0 & otherwise \end{cases} \tag{3.15}$$

The logic condition $|p_{chassis}^{\pm}| \geq |p_{cueing}^{\pm}|$ prevents an unexpected change of sign in the difference between the two signals. Then the two computed signals p_0^+ and p_0^- are merged, and the reference contact pressure signal p_0 is obtained. This active strategy takes into account the inconsistencies between the two lateral models and computes a reference signal without discontinuities.

3.3 MPC control

Another strategy to replicate the real car sensations in the simulator is the tracking of the somatosensory pressure, the pressure perceived by the driver. In the proposed control scheme, shown in 3.7, exploiting the model predictive control framework (MPC), the computation of the contact reference signals is achieved through an optimization technique. The prediction of the model states of the MPC allows to compute the control signal as function of the predicted perceived pressure.
Moreover, the actuators of the active seat bladders presents an intrinsic delay, that must be taken into account in the system dynamic.

3.3.1 Tactile adaptation

Tactile adaptation is a phenomenon of the sensory system that results in temporal desensitization after an exposure to sustained or repetitive tactile stimuli. In [19], a decreasing brain activity has been highlighted during a sustained pressure stimulus on the fingertip, and conse-

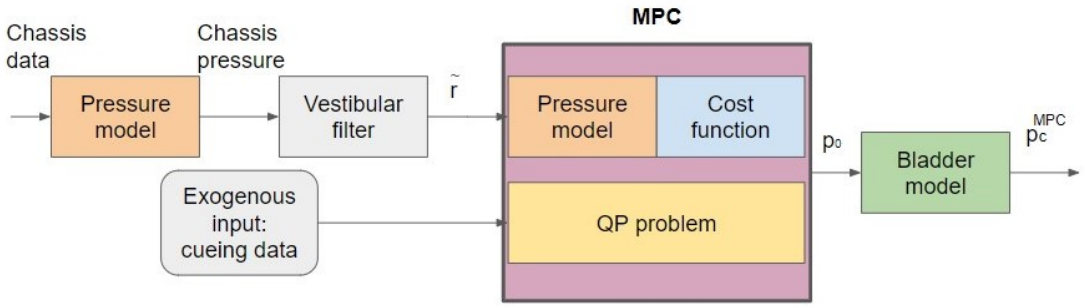

Figure 3.7: MPC control scheme

quently a parametrization is proposed. The brain activity of every voxel (volumetric unit of the brain) has been estimated through its oxygenation level: the higher the oxygenation level, the more the brain activity. The MRI scan marks with different colors different oxygenation levels. As stated in [20], the regions of interest (ROI) for the tactile stimuli are cBA1, cBA2,

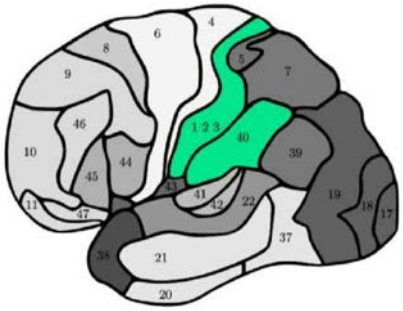

Figure 3.8: Brain ROIs

and cBA3 on the primary somatosensory cortex, and cBA40 on the secondary somatosensory cortex. The four ROIs are shown in figure 3.8 and identified by labels $1 - 2 - 3 - 40$ respectively.

In figure 3.9 three MRI scans shows the decreasing voxels activity during a sustained pressure stimulus.

There is an adaptation process in the perception mechanism aimed to maintain active only

the brain regions effectively connected to the particular tactile stimulation. In [19] a model has been developed to relate the number of active voxels y and the time duration t of the tactile stimulus:

$$y = ce^{\alpha_0 + \tau t} \tag{3.16}$$

where c and α_0 are constant parameters, and τ the system time constant. In figure 3.10, relation 3.16 is shown with the identified parameters for every considered ROI. The identified

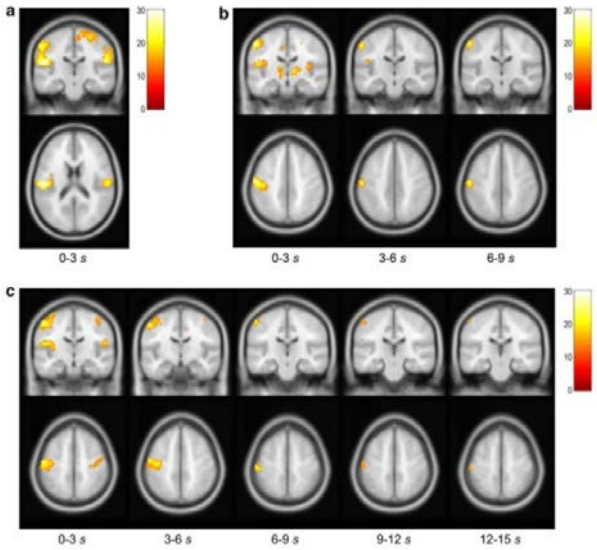

Figure 3.9: MRI Scans at different time intervals during a pressure stimulus applied on the fingertip

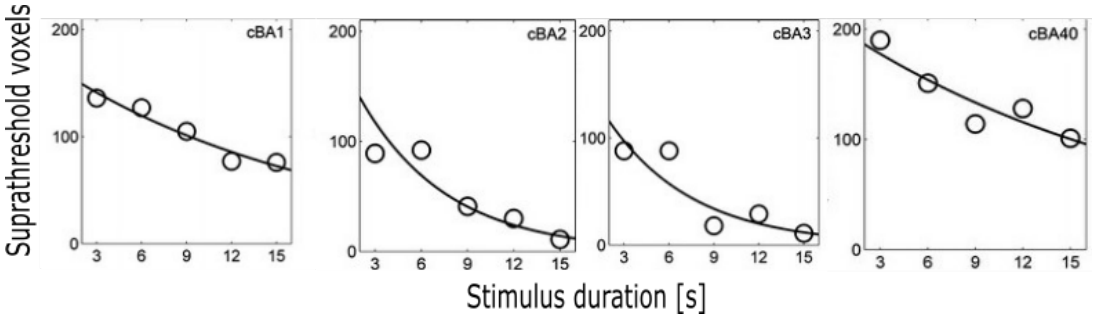

Figure 3.10: Active voxels number decaying with respect to the stimulus duration

time constants are reported in table 3.3.1. To model the tactile adaptation behavior, an high pass filter has been implemented with time constant $\tau_{hp} = 20.99[s]$, corresponding to a cut

ROI	τ
cBA3	5.69
cBA1	18.03
cBA2	5.66
cBA40	20.99

Table 3.1: Time constants τ for the considered ROIs

frequency of $f_{hp} \approx 0.048[Hz]$. We can express this filter as:

$$W_{hp}(s) = \frac{\tau_{hp} s}{1 + \tau_{hp} s} = 1 - \frac{\frac{1}{\tau_{hp}}}{\frac{1}{\tau_{hp}} + s} \tag{3.17}$$

Denoting p a generic physical pressure, applied on the driver's body, the corresponding perceived pressure $\bar{p}$ can be computed applying the filter 3.17.
A realization of 3.17 is:

$$\begin{cases} \dot{x}_p = -\frac{1}{\tau_{hp}} x_p + \dot{p} \\ \bar{p} = x_p \end{cases} \tag{3.18}$$

3.3.2 Electro-pneumatic actuator dynamics

The active seat bladders are actuated by electro-pneumatic valves, controlling the pneumatic compressor airflow. The valves, installed in the considered active seat, are electro-pneumatic proportional VPPX valves built by FESTO, with settling time at the reference pressure of $100[ms]$.
A low pass filter is used to model the delay of the actuators. The relative transfer function is the following:

$$W_{lp}(s) = \frac{1}{1 + \tau_{lp} s} \tag{3.19}$$

with $\tau_{lp} = 0.1[s]$. A state system realization of 3.19 is:

$$\begin{cases} \dot{x}_v = -\frac{1}{\tau_v + \dot{p}_0} \\ \hat{p}_0 = x_v \end{cases} \tag{3.20}$$

where p_0 is the reference contact pressure and $\hat{p}_0$ is its delayed and filtered version. The signal $\hat{p}_0$ embedding the actuators delay, applied as input of the inflatable bladder model in 2.34,

allows the computation of the inner bladder pressure that the driver would be subjected to on a real active seat.

3.3.3 MPC for somatosensory reference tracking and actuators delay compensation

The developed model receives in input the reference signal $\tilde{r} = \hat{p}_{chassis}$, the perceived pressure in the real car, and computes, as output, the contact pressure $\hat{p}_0$ of the active seat bladders.

The control signal $\dot{p}_0$ is the variation of the contact pressure provided by the bladders. The latter is computed by MPC, aiming at minimizing the perceived pressure error between the real car and the simulator. The dynamic of the actuators is taken into account imposing the same dynamic to the state variable $\hat{p}_0$.
The signal $\hat{p}_0$ is then used, in combination with the driver's trunk displacement, to compute the control signals for the actuators of the Active Seat by exploiting the inflatable bladder model in section 2.4.

Lateral pressure model for MPC

For the lateral pressure model, starting from the expanded lateral model in 3.10, considering the tactile adaptation and the actuators delay we get:

$$\begin{cases} \ddot{d}_y & = a_{y,drv} - \frac{K(d_y)d_y}{m} - \frac{C(d_y)\dot{d_y}}{m} - \frac{F_{fric}}{m} + \frac{F_{tilt,y}}{m} + \frac{F_{grav}}{m} \\ \dot{z} & = \dot{d}_y - \frac{|d_y|}{h(d_y)}\dot{d}_y \\ \dot{\hat{p}}_{0,lat} & = -\frac{1}{\tau_{lp}}\hat{p}_{0,lat} + \dot{p}_{0,lat} \\ \dot{\bar{p}}_{s,lat} & = -\frac{1}{\tau_{hp}}\bar{p}_{s,lat} + \dot{y}_{p,lat} \end{cases} \tag{3.21}$$

where:

$$
\begin{aligned}
y_{p,lat} &= p'_{lat} + \hat{p}_{0,lat} \\
K(d_y) &= k_2 d_y^2 + k_0 \\
C(d_y, \dot{d}_y) &= c_{seat}^{hyst}(d_y, \dot{d}_y) + c_0 \\
F_{fric} &= \sigma_0 z + \sigma_1 \frac{dz}{dt} \\
F_{tilt,y} &= -mg \sin(\phi) \\
F_{grav} &= Mg \sin(\beta(d_y)) \cos(\beta(d_y)) \\
h(\dot{d}_y) &= F_d + (F_s - F_d)\, e^{\left(\dot{d}_y / v_s\right)^2} \\
F_s &= \mu_s N \\
F_d &= \mu_d N \\
N &= ma_x \cos(\alpha) + Mg \sin(\alpha).
\end{aligned}
$$

In the previous equations d_y, $\dot{d}_y$, and $\ddot{d}_y$ represents the driver's trunk lateral dynamic, and $\dot{y}_{p,lat}$ is the derivative of the overall lateral pressure on the driver's trunk, computed as sum of 3.9 and the active seat contact pressure $\hat{p}_{0,lat}$. The state variable $\bar{p}_{s,lat}$ is the somatosensory perceived pressure on the lateral driver's trunk. The exogenous inputs of the model are the same of model 3.10: the lateral driver acceleration, the platform longitudinal acceleration, and the platform roll.

4

Enhanced haptic feedback

In this chapter, we start from the actual control scheme of the Active Seat, which is described in section 2.2, and we study different strategies to enhance the haptic feedback framework. The objective is to define a pressure model to take into account the pressure induced by the platform movement in the generation of the pressure cues on the driver. In the first part, under the hypothesis that the driver is integrated with the seat, two different models are proposed to compute the driver's trunk pressure. At the end of this chapter, exploiting the lateral models of section 4.1, the feedforward control scheme of section 3.2 is adapted to compute the control signals in the haptic feedback framework.

4.1 Lateral pressure model for the haptic feedback

The lateral model, characterized in this section, describes the pressure exerted between the driver's trunk and the lateral sides of the seat. The model describes the pressure both in a real car scenario and in a dynamic driving simulator. In the following, only the lateral pressure is taken into account as the longitudinal pressure can be described through a similar model. The vertical model, has been neglected, since vertical forces are not so remarkable in the description of pressure. Recalling the lateral model described in section 2.3 and assuming that the driver is integrated with the seat we can rewrite the problem without the driver's trunk displacement. The forces, applied on the driver's center of mass, do not contribute to the driver's trunk dynamic but affect the lateral pressure directly with the seat. The driver

is modeled as an homogeneous rod of length L and mass M, fixed on the seat. The inertial mass of the driver's trunk is still m, as computed in section 2.3.1. Due to the seat acceleration in the world reference frame, the external lateral force acting on the driver is:

$$F_{ext} = ma_{y,drv} \tag{4.1}$$

The tilt inclination of the seat has an important role in the driver's perception as discussed in section 2.3.3. The roll dynamic of the seat produce a force on the driver's that can be expressed as:

$$F_{tilt,y} = -mg\phi \tag{4.2}$$

where ϕ is the roll angle of the seat in the world reference frame. The overall force acting on the driver can be written as:

$$F_{tot,lat} = F_{ext} + F_{tilt,y}. \tag{4.3}$$

Since there is no movement, between the driver and the seat, the reaction force between the side of the seat and the driver's trunk is equal, in magnitude, to 4.3. By definition, we can compute the lateral pressure on the driver's trunk as:

$$p^*_{lat} = \frac{F_{tot,lat}}{A} \tag{4.4}$$

where A is the contact area.

4.1.1 The filtered model

The high-frequency components of the acceleration signals are not informative for the active seat, on the contrary, these components are detrimental for the control signals computation of the active seat. The system aims to reproduce the pressure induced by low-frequency accelerations exerting an haptic feedback on the driver's body.

A low-pass Butterworth filter is developed to remove the high frequency component, the filter cut-off frequency is a tunable parameter of the model. The low-pass filtered accelerations can be applied as input to the model proposed in the previous section to obtain the

filtered lateral pressure:

$$\begin{cases} \hat{F}_{ext} = m\hat{a}_{y,drv} \\ F_{tilt,y} = -mg\phi \\ \hat{F}_{tot,lat} = \hat{F}_{ext} + F_{tilt,y} \end{cases} \quad \Rightarrow \quad \hat{p}^*_{lat} = \frac{\hat{F}_{tot,lat}}{A} \tag{4.5}$$

4.2 Control schemes for enhanced haptic feedback

4.2.1 Enhanced actual control strategy

We recall the actual control strategy of the active seat discussed in section 2.2. Starting from the real car acceleration, the control signals for the active seat are computed through a filtering stage and some signal processing. The bladders are used to create an haptic feedback of the accelerations. In the following we will focus on the lateral pressure of the driver's trunk, hence on the control of cushions 2 and 5 in figure 2.1.
Differently from the actual control, the pressure induced by the platform movement is taken into account exploiting model 4.4 or 4.5. The output of the lateral model is divided in positive and negative part. The pressure is directly connected to the accelerations signals because of the assumption that the driver is integrated with the seat. The main aim is to compute the inner pressure of the bladders, corresponding to the contact pressure induced by the platform movement, and to remove this quantities from the corresponding outputs of the actual control scheme. The result is the pressure of the real car acceleration minus the contribution of the pressure induced by the simulator movement multiplied by a proportional term for the contact/inner pressure conversion of the bladder. For bladder 2, we can be write:

$$p^*_{c,left} = p^{VI}_{c,left} - Vp^+_{lat} \tag{4.6}$$

where V is a suitable converting gain contact/inner pressure and p^+_{lat} is the positive part of p^*_{lat} or $\hat{p}^*_{lat}$, depending on the selected lateral model. For the right bladder the solution is symmetrical. A lower saturation is applied to the outputs of the control system to prevent the output pressures to be lower than a minimum value. The control scheme of the system is shown in 4.1.

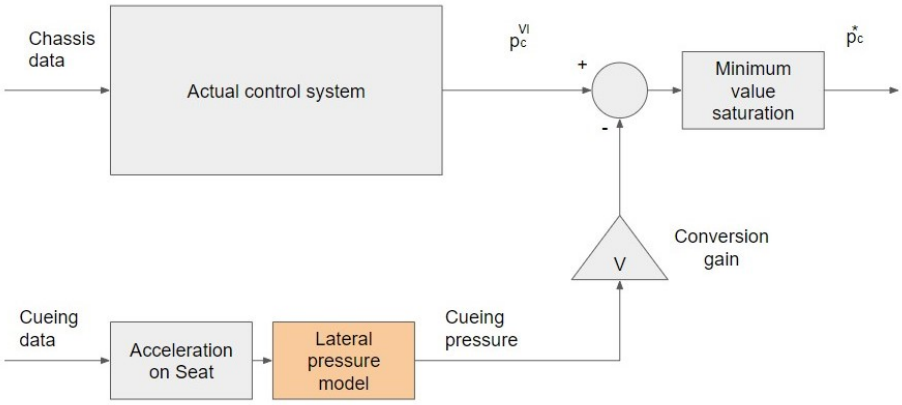

Figure 4.1: Enhanced actual control scheme

4.2.2 Feedforward control

The second solution is based on the feedforward control scheme of section 3.2. Considering one of the two models of section 4.1, we can compute the pressure between the driver's trunk and the seat, both in the real vehicle and in the simulator. Under the assumption of the driver integrated with the seat, the computed pressure is directly connected to the acceleration. The Active seat policies, explained in section 3.2.1, are implemented to handle the possible inconsistencies between the output pressures of the two lateral models. Then, the contact pressure p_0 between the driver's trunk and the bladders is computed. The inner pressure of the bladders, $p_c^{*,FF}$, is obtained by exploiting the inflatable bladder model of section 2.4, assuming zero the driver's displacement on the seat.

5
Results

In this chapter, the experimental results obtained during a professional driver training session on a simulator platform are reported. Thanks to VI-grade collaboration, data concerning several driving sessions have been used to simulate the behavior of the active seat in a dynamic driving simulator. The virtual track considered is a digital version of the *Calabogie MotorSports Park* (Ontario, CA). The map of the track is shown in figure 5.1.

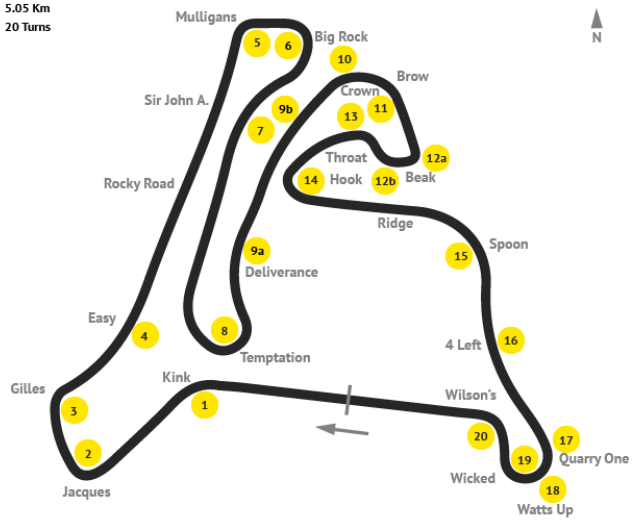

Figure 5.1: Calabogie MotorSports Park track

Given the huge amount of data, in the following discussion only the first $30[s]$ of the track are considered. This section of the track is chosen because of the presence of 4 turns, 2 for each side, with different curve radii and with different longitudinal speeds. The accelerations data and the angles dynamics are shown in figures 5.2 and 5.3, both for the real vehicle and the simulator platform.

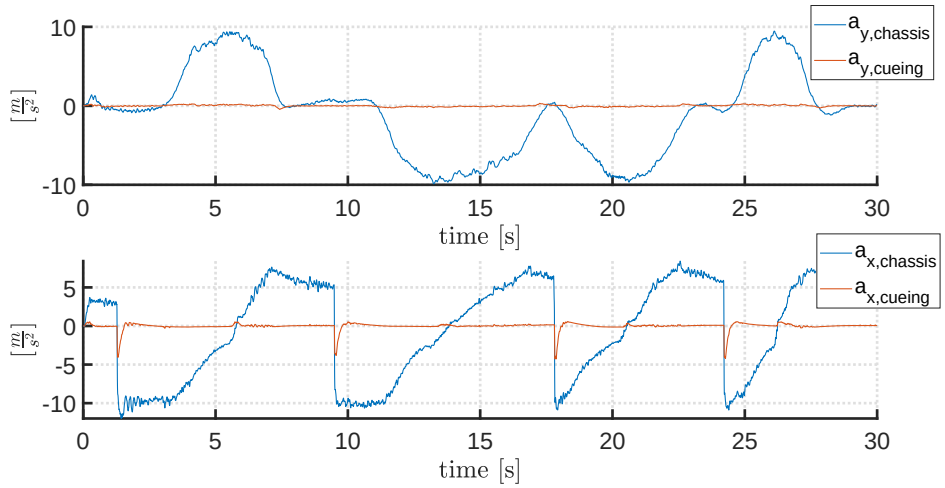

Figure 5.2: Comparison between accelerations of the real car and the simulator in Calabogie MotorSports Park track

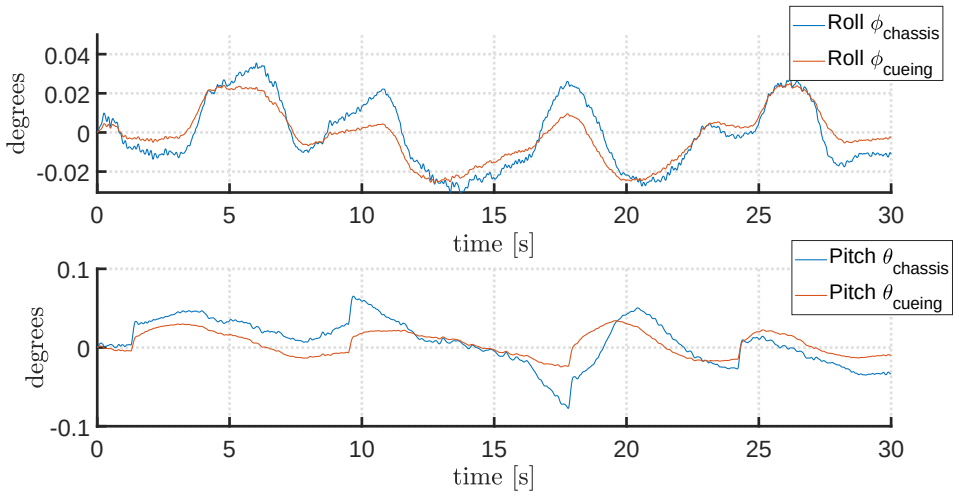

Figure 5.3: Comparison between roll and pitch angles of the real car and the simulator in Calabogie MotorSports Park track

5.1 Lateral pressure models

5.1.1 Lateral pressure model based on the driver's displacement on the seat

In this section, we focus on the differences between the lateral model discussed in 2.3 and its enhanced version of section 3.1. The main differences are the introduction of the hysteresis function on the damping component of the seat and of the contribution of the gravity force on the driver's dynamic. The comparison between model 2.16 and the extended model 3.10 is shown in figure 5.4 for the real vehicle scenario and in figure 5.5 for the simulator platform. Both figures represents the lateral contact pressure between the driver's trunk and the seat in the first $30[s]$ of the Calabogie track.

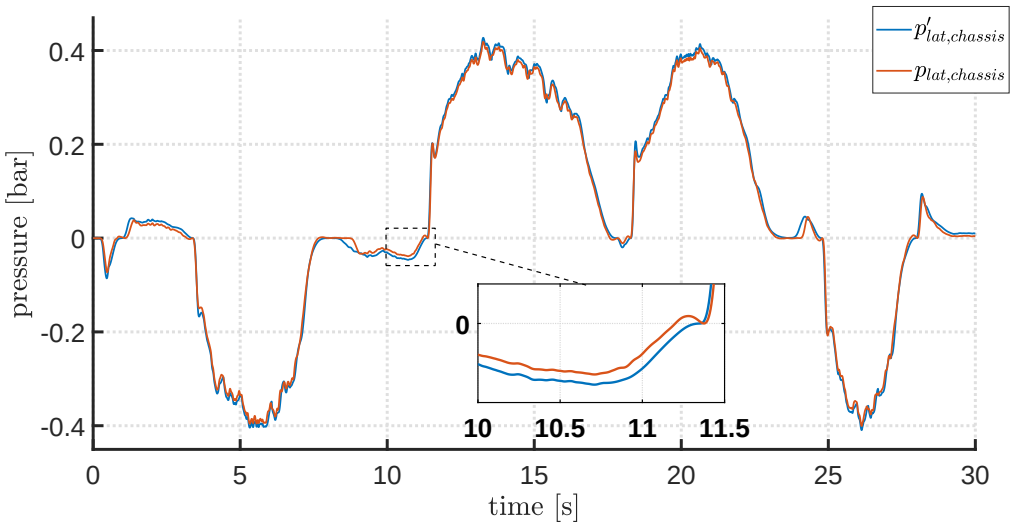

Figure 5.4: Comparison between the lateral pressure $p'_{lat,chassis}$ computed by the extended model 3.10 and $p_{lat,chassis}$ computed by model 2.16 in the real vehicle.

The introduction of the hysteresis function on the damping component of the seat c^{hyst}_{seat}, discussed in section 3.1.1, have two major consequences. The first effect is to remove the pressure peaks when the driver's body is moving toward the center of the seat, as can be seen in the zoomed section of figure 5.4. The second consequence is a slight amplification of the peaks that are due to the impact between the driver's trunk and the side of the seat. In the expanded model, the driver's body reaches an higher velocity in the zero-damping regions. When the impact occurs, the seat damping reaction force $F_{damp} = c^{hyst}_{seat}(d_y, \dot{d}_y)\dot{d}_y$ shows a peak, corresponding to the increase of the reaction force of the seat, slowing down the driver's body.

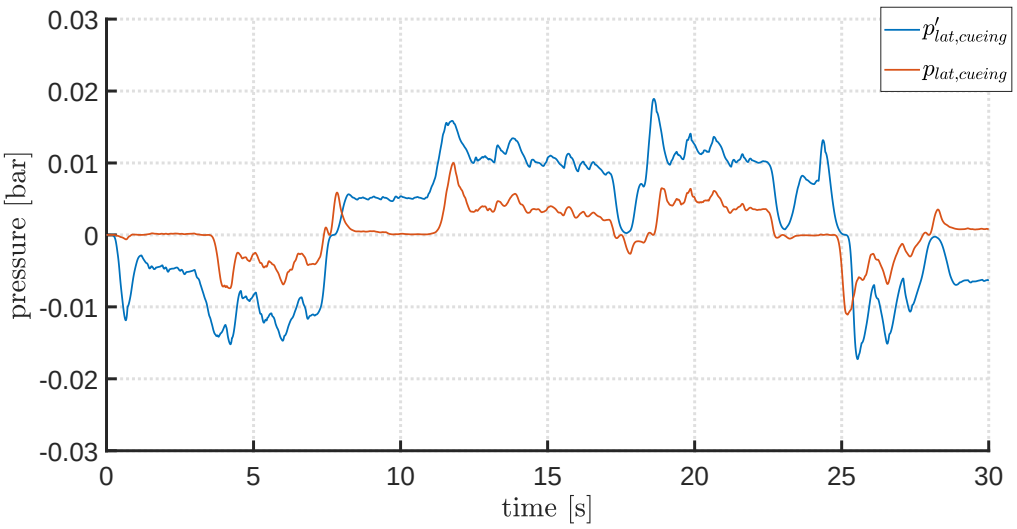

Figure 5.5: Comparison between the lateral pressure $p'_{lat,cueing}$ computed by the extended model 3.10 and $p_{lat,cueing}$ computed by model 2.16 on the simulator platform.

Since the reaction force of the seat is directly connected to the lateral pressure, by relation 3.9, we have a peak also in the lateral contact pressure.

In the expanded model 3.10, the gravity force component is considered in the computation of the driver's trunk dynamic, as explained in section 3.1.2. The effect of the gravity force on the lateral dynamic is not so remarkable in the real vehicle, although we can notice some differences in the pressure outside the four main turns.However, the main effect of the introduction of the gravity component is visible in figure 5.5. On the simulator platform, the accelerations have a lower magnitude with respect to the real car, so the effect of the gravity is fundamental to describe the driver's movement on the seat.

A limit of the lateral model is its high sensitivity on the model parameters: small changes in their values can lead to completely different outputs. This aspect could make the model calibration difficult in a real test.

5.1.2 Lateral pressure models of a driver integrated with the seat

In section 4.1, two models are proposed for the computation of the lateral pressure between the driver's trunk and the seat. These models are derived from model 3.10, under the assumption of a driver integrated with the seat. This strong assumption allows to compute a lateral pressure directly linked to the acceleration signal. This feature is interesting for the realiza-

tion of the haptic feedback strategy. The input signals are shown in figure 5.2 and in figure 5.3. Exploiting the models of section 4.1, the computed pressure outputs are shown in figure 5.6 for the real vehicle, and in figure 5.7 for the simulator case. In the following results, the cut-off frequency of the low-pass filter has been chosen as $f_{fm} = 62.8[Hz]$.

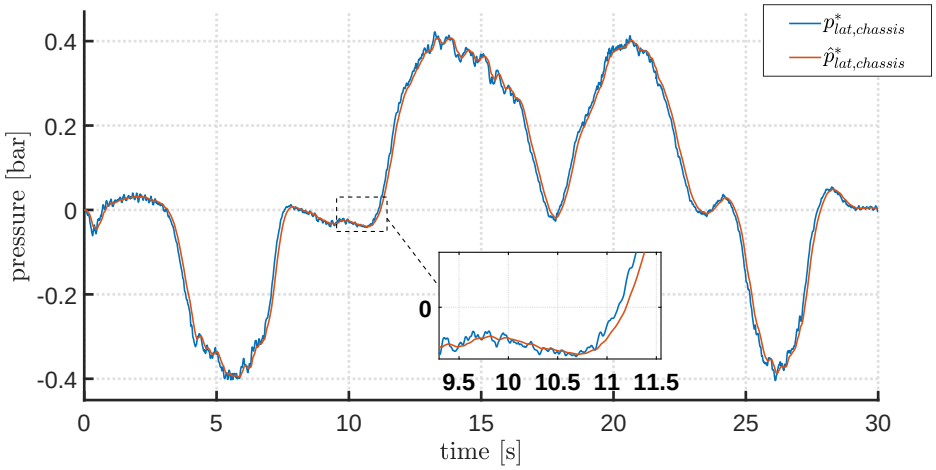

Figure 5.6: Comparison between the lateral pressure $p^*_{lat,chassis}$, computed by model 4.4 and its filtered version $\hat{p}^*_{lat,chassis}$ computed by model 4.5 in the real vehicle.

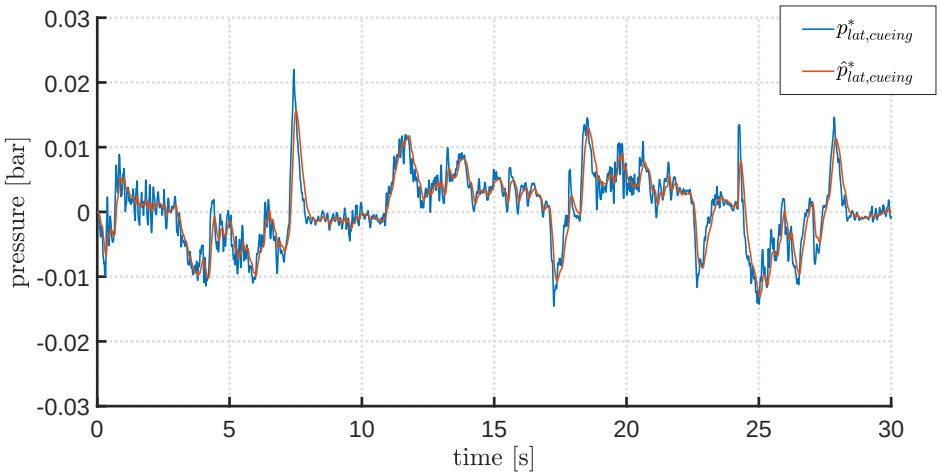

Figure 5.7: Comparison between the lateral pressure $p^*_{lat,chassis}$, computed by model 4.4 and its filtered version $\hat{p}^*_{lat,chassis}$ computed by model 4.5 on the simulator.

As expected, the filtered model 4.5 computes a smoother and delayed version of the lateral pressure computed by the model 4.4. The direct link between the pressure and the acceleration comports a low capability in the description of low-frequency components of the pressure. This can be easily seen in figure 5.7. The introduction of a small delay in the output of model 4.5, due to the low-pass filtering, seems an acceptable trade-off to remove the high-frequency noise.

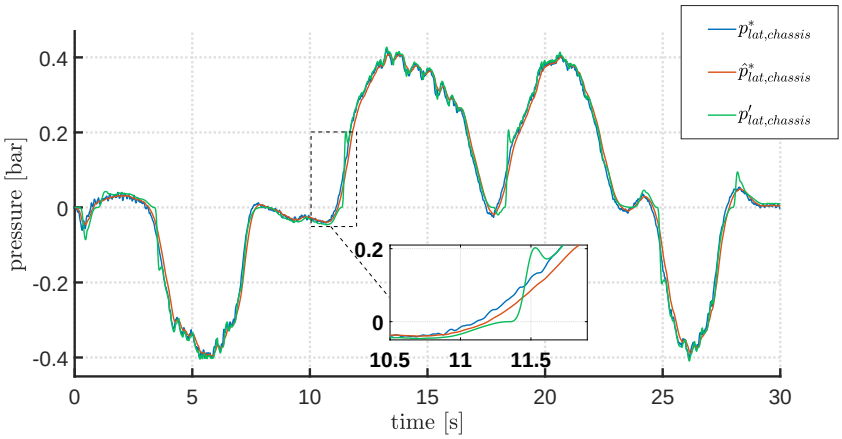

Figure 5.8: Comparison between the lateral pressure $p^*_{lat,chassis}$ computed with model 4.4, $\hat{p}^*_{lat,chassis}$ computed by model 4.5, and $p'_{lat,chassis}$ computed exploiting the extended lateral model 3.10 in the real vehicle.

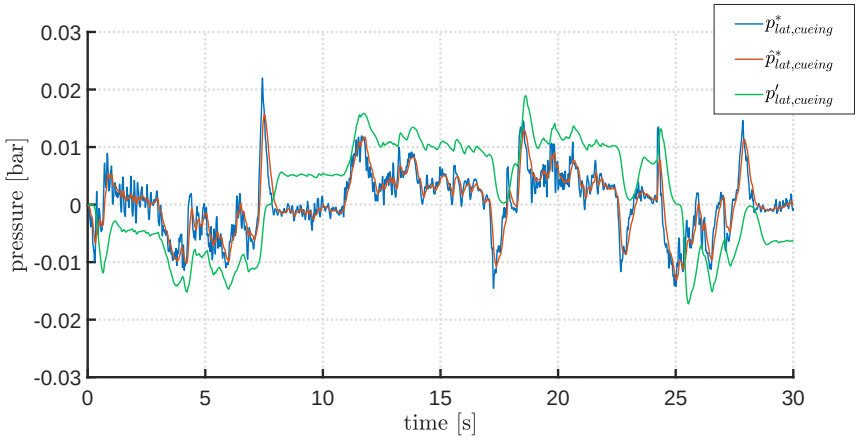

Figure 5.9: Comparison between the lateral pressure $p^*_{lat,chassis}$ computed with model 4.4, $\hat{p}^*_{lat,chassis}$ computed by model 4.5, and $p'_{lat,chassis}$ computed exploiting the extended lateral model 3.10 on the simulator.

The comparison between the lateral pressures, computed with the models of section 4.1

and the extended model 3.10, is shown in figures 5.8 and 5.9. The output signal of the extended lateral model 3.10, where the output pressure relies on by the driver's displacement, is delayed with respect to the other models. This delay is due to the travel time of the body on the seat. Moreover, the impact between the driver and the seat is not considered in the models 4.4 and 4.5, hence the absence of the peaks in the output pressures during the initial phase of a turn. Another important aspect, visible in figure 5.9, is the higher description capability of model 3.10 of the low-frequency components that can not be directly derived from the acceleration signals.

5.2 Model-based pressure cues strategy

5.2.1 Feedforward control

In section 3.2 a control scheme for the active seat system is introduced. This feedforward control strategy exploits model 3.10 to compute the lateral contact pressure between the driver and the seat. The control system aims at reproducing the same pressure cue the driver would feel in the real vehicle, hence the bladders of the active seat should compensate for the lacking pressure due to the movement constraints of the simulator platform. The desired contact pressure between the driver and the bladders is computed exploiting the compensation policies of section 3.2.1 and consequently the inner pressure of the bladders is obtained with the model described in section 2.4. As follows such a control strategy is analyzed in the fist $30[s]$ of the Calabogie track.

The Active Seat compensation policies comparison

First of all, the comparison between the proposed strategies is proposed. In figure 5.10, the desired contact pressure between the driver and the bladders 2 and 5 of figure 2.1 is computed adopting all three different strategies, starting from the contact pressure signals between the driver and the seat in the real vehicle and in the simulator.

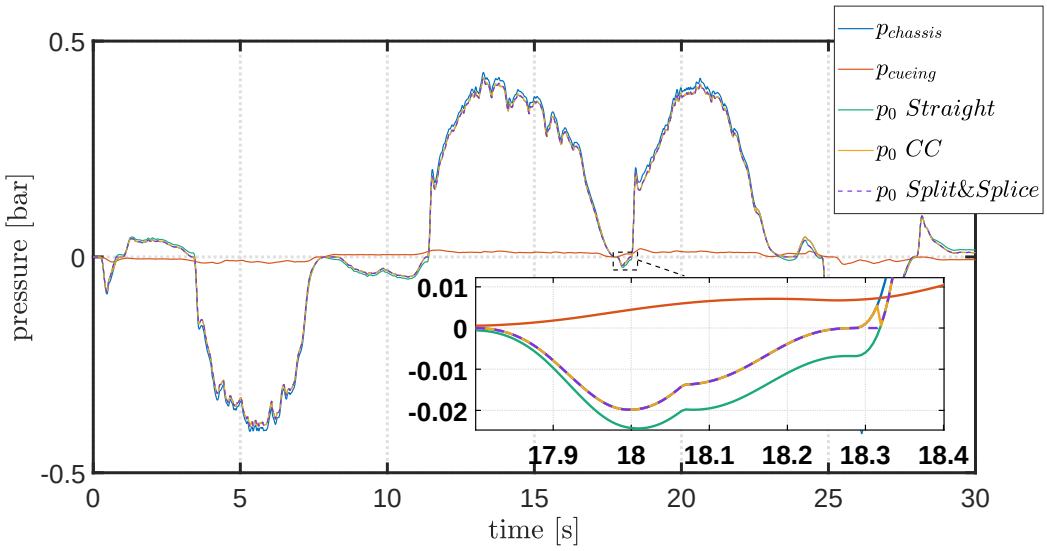

Figure 5.10: Comparison of the Active Seat compensation policies in the computation of the desired contact pressure signal between the driver and the bladders.

In figure 5.10, it can be observed that the *Straight* strategy often computes a desired contact pressure for the bladders higher than the actual pressure in the real car. This problem arises from the different signs of the computed pressures in the simulator and in the real vehicle. The *Consistency Conditions* strategy instead, prevent the overestimation problem, but the set of logic conditions 3.14 introduces some discontinuities, in particular when one of the input signals crosses the zero value. On the contrary, the $Split\&Splice$ policy, in which the reference contact pressure is computed separately for every bladder, can handle smoothly both the inputs change of sign and the cases when the computed contact pressures are on different sides of the seat.

In the following the $Split\&Splice$ policy will be adopted as the default active seat compensation policy since it provides the best output signal without any downside.

Simulative results

In this section, the results of the feedforward scheme are reported and analyzed. In the first plot of figure 5.11, the lateral accelerations on the driver in the real car and in the simulator platform are shown. In the second plot of figure 5.11 instead, the output pressures between the driver and the seat, computed exploiting model 3.10, are shown.

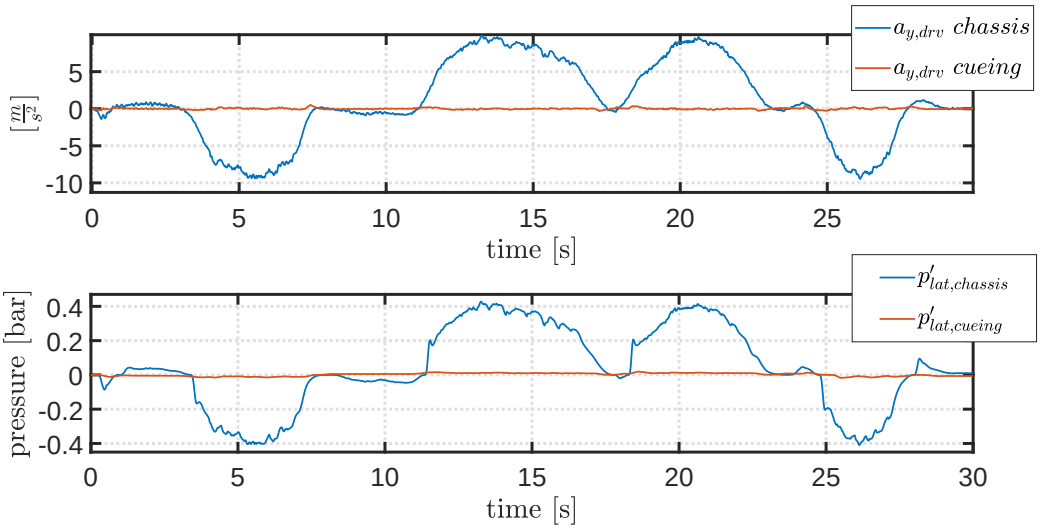

Figure 5.11: In the first plot the input accelerations of the driver with respect to the seat, in the second plot the corresponding computed pressures exploiting model 3.10.

From the lateral pressures, in the two considered cases, applying the *Split&Splice* compensation policy we obtain the desired contact pressure p_0 between the driver and the bladders, as can be seen in figure 5.12.

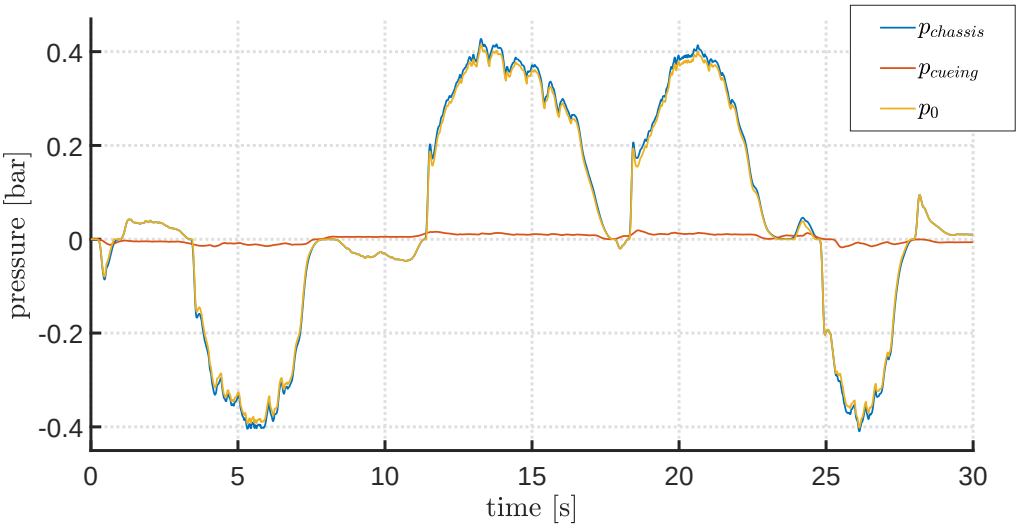

Figure 5.12: The desired contact pressure p_0 between the driver and the bladders starting from the computed lateral pressures using model 3.10 in the real vehicle and in the simulator

From the computed desired contact pressure p_0 and the driver's lateral displacement on the seat, the inner pressure of the bladders can be computed using the model described in section 2.4.

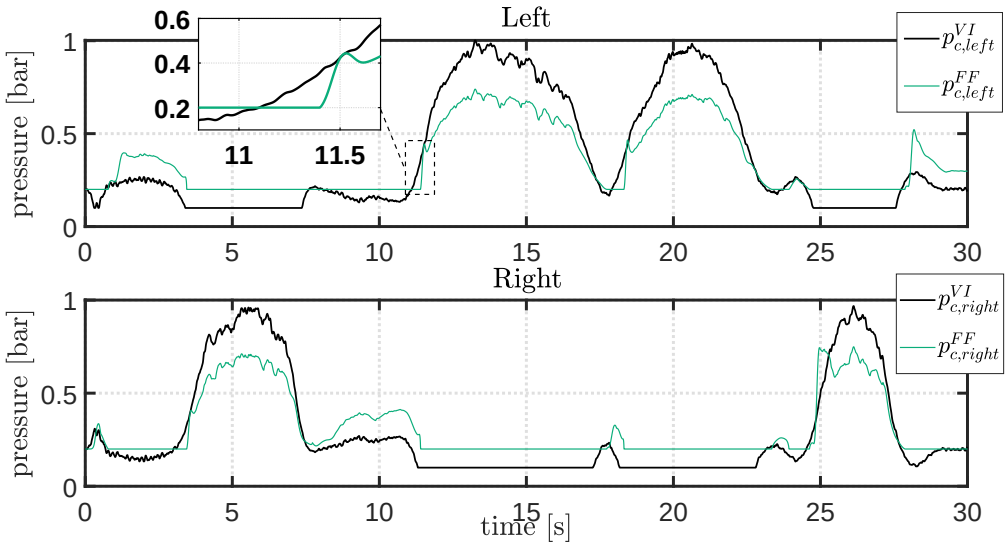

Figure 5.13: Comparison between the inner pressure of the bladders 2 and 5 of figure 2.1. The green signal p_c^{FF} is computed exploiting the feedforward control scheme of figure 3.6, the black signal p_c^{VI} is the inner pressure computed by the actual control of section 2.2.

The computed inner pressure of the bladders, shown in 5.13, exerts on the driver's trunk the desired contact pressure p_0 to trick the driver's somatosensory system to perceive the same pressure cue as if it was in the real vehicle. The inner bladder pressure is supposed to have an offset pressure of $0.2[bar]$ as the real bladders mounted on the Active seat system. The inner pressures of the bladders computed by the actual control of section 2.2 are also shown in figure 5.13. We can notice that the output of the feedforward control p_c^{FF} follows the trend of the desired contact pressure p_0. In the model-based pressure cue framework, because of the pressure dependency on the driver's displacement, the bladders inflates with a slight delay with respect to p_c^{VI}, computed by the actual control. This delay is tied to the time that takes the body to move from one side of the seat to the other, in this small interval of time the driver is not feeling pressure in the moving direction. Moreover, in the first part of a turn, the pressure cue is induced by the platform movement and then, the bladders inflate to sustain the pressure cue on the driver. The difference in magnitude, between the two approaches, is highly influenced by the choice of the tunable parameters in the actual control and hence

not so informative.

The presence of some peaks in p_c^{FF} is due to the assumption of instant contact between the driver and the cushions. To partially avoid this phenomenon, the driver displacement is saturated at the zero value for every bladder. Although the limited tracking horizon, the bladders inflates as soon as the driver's trunk center of mass pass trough the zero value, causing the pressure peak. This assumption of instant contact between driver and cushions and the consequent tracking behavior of the bladders could be a problem in a real test on the simulator. In fact, small errors in the computation of the driver's lateral displacement or the contact pressure, could lead to some false pressure cues on the driver's trunk ruining the driving experience. To assert the feasibility of this strategy, a test on a real dynamic simulator with a professional driver is required.

5.2.2 MPC control

In section 3.3, the MPC control is proposed to track the perceived reference lateral pressure on the driver's trunk in the real car vehicle. The MPC computes the control signal $\dot{p}_0$, variation of the contact pressure provided by the bladders, minimizing the perceived pressure error between the real car and the simulator. The dynamic of the actuators is taken into account imposing the same dynamic to the state variable $\hat{p}_0$.

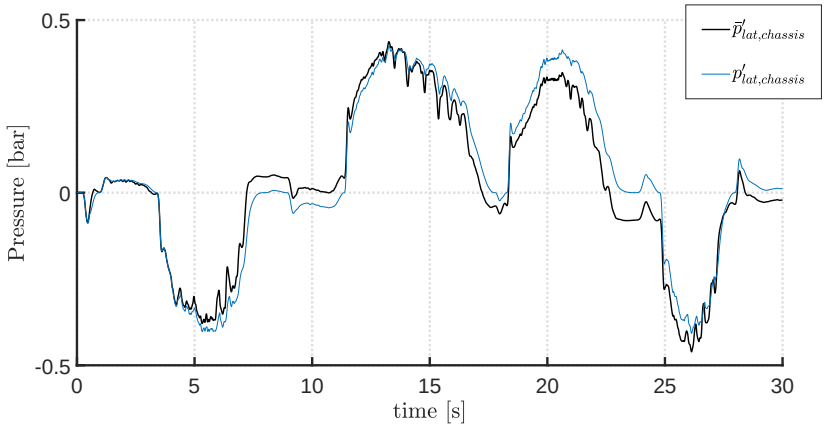

Figure 5.14: Comparison between the pressure on the real car $p'_{s,chassis}$, output of model 3.10, and the corresponding perceived pressure $\bar{p}'_{s,chassis}$ obtained filtering with 3.17.

In figure 5.14 the perceived pressure on the real vehicle is shown, obtained applying the

filter 3.17 and modeling the tactile adaptation discussed in section 3.3.1. The implementation of the model 3.21 in the MPC framework exploit the MATMPC tool, developed in [21].

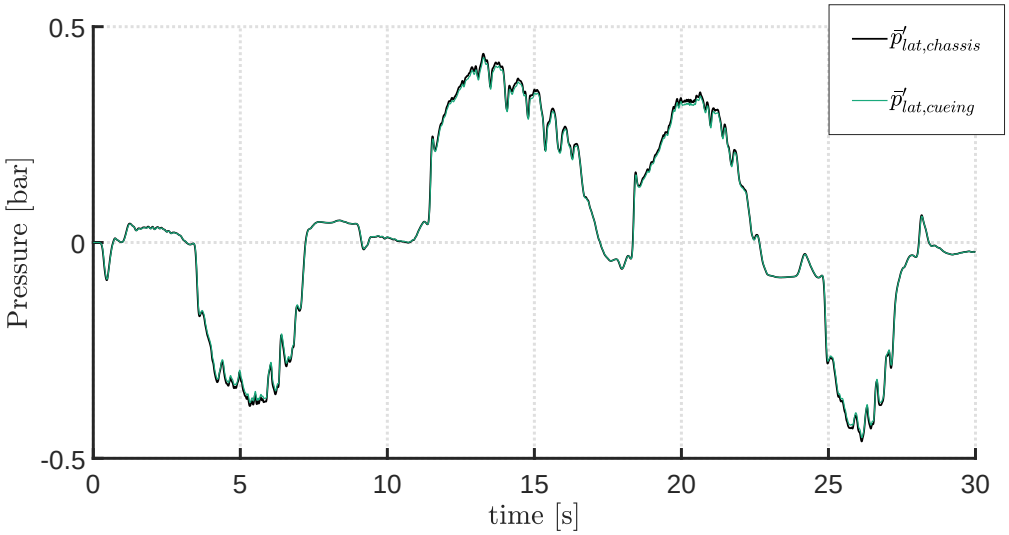

Figure 5.15: Comparison between the perceived lateral pressure in the real vehicle $\bar{p}'_{lat,chassis}$, computed filtering with 3.17 the output of model 3.10, and in the simulator $\bar{p}'_{lat,cueing}$, output of the MPC scheme (in figure 3.7).

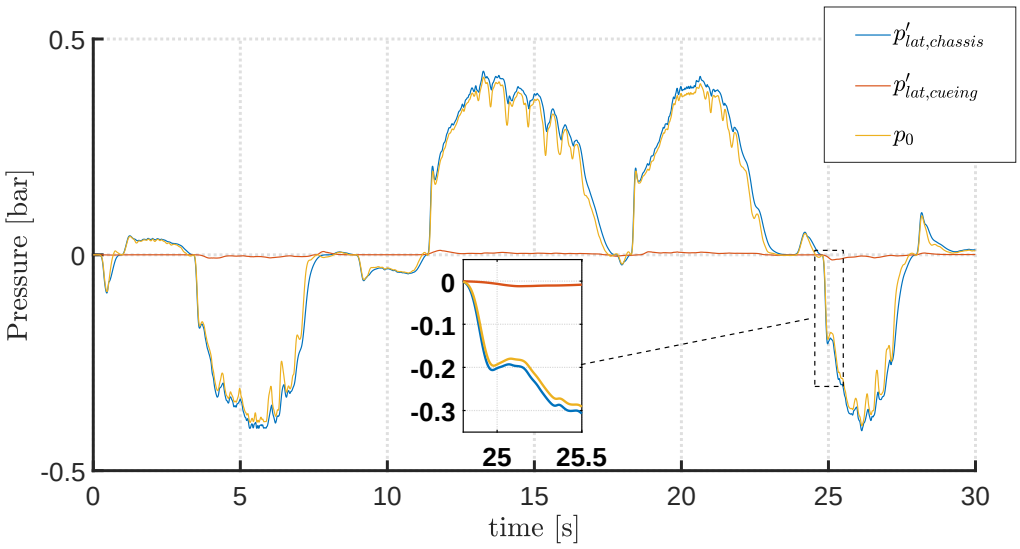

Figure 5.16: Lateral pressure computed with the MPC scheme: $p'_{lat,chassis}$ is the pressure on the real vehicle, $p'_{lat,cueing}$ is the pressure induced by the platform movement, and p_0 is the desired contact pressure between the driver and the bladders to reproduce the perceived pressure in the real car.

As can be seen in figure 5.15, the control system achieves a good tracking of the reference signal: the overall perceived lateral pressure on the simulator is very close to the perceived pressure in the real car. It is interesting to notice, in figure 5.16, that to minimize the error between the two perceived pressures, the sum of the computed desired contact pressure between the driver and the bladders p_0 and the pressure induced by the platform movement $p'_{lat,cueing}$ is almost equal to the overall physical pressure on the real vehicle $p'_{lat,chassis}$.

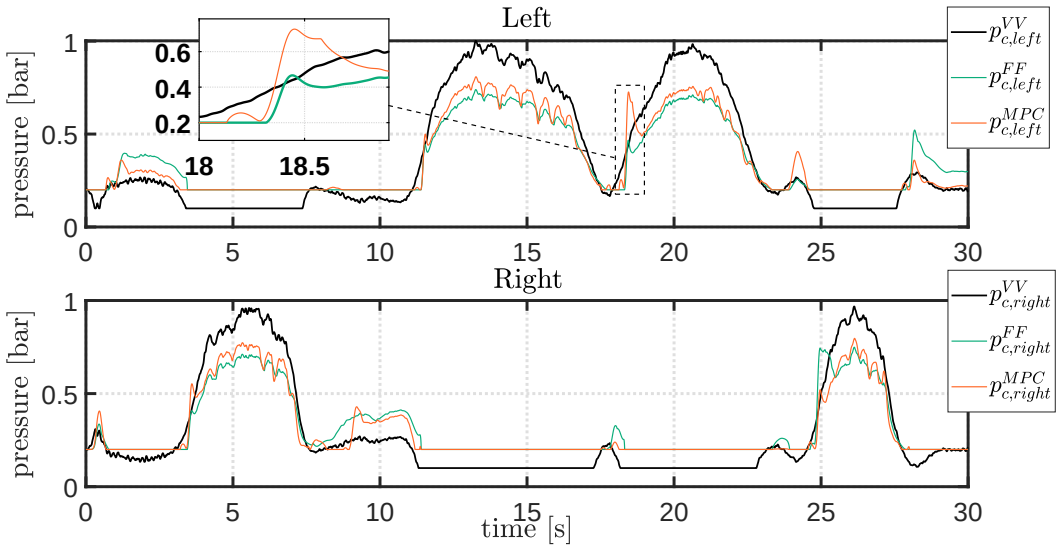

Figure 5.17: Comparison of the computed inner pressures of the bladders 2 and 5 of figure 2.1: p_c^{MPC} (in orange) exploiting the MPC scheme of section 3.3, p_c^{FF} (in green) computed with the feedforward scheme of section 3.2, and p_c^{VI} (in black) obtained with the actual control of section 2.2.

The computed inner pressure of the bladders, shown in figure 5.17, exerts on the driver's trunk the desired contact pressure p_0 to cheat the driver's somatosensory system to perceive the same pressure cue as in the real vehicle. The inner bladder pressure is supposed to have an offset pressure of $0.2[bar]$ as the real bladders mounted on the Active seat system. The inner pressure of the bladders computed by the actual control of section 2.2 and the results obtained with the feedforward scheme are also show in figure 5.17. We can notice that the output of the MPC scheme, p_c^{MPC}, follows the trend of the desired contact pressure p_0. The MPC control takes into account the delay of the actuators of the active seat, this can be noticed in the picture-in-picture of figure 5.17 where the pressure signal is slightly anticipating p_c^{FF}. All the observations made on the inner pressure of the bladders in section 5.2.1 hold

also in the case of the MPC scheme. We can notice that the peaks due to the tracking effect of the bladders are further amplified in some cases.

5.3 Control strategies for haptic feedback

The control schemes, developed in section 4.2, aim to take into account the pressure induced by the platform movement in the generation of an haptic feedback for the driver. This feedback must be informative on the magnitude and the direction of the desired acceleration the driver should perceive.

5.3.1 Enhanced version of the actual control scheme

The actual control, described in section 2.2, starting from the real car accelerations computes the control outputs, shown in figure 5.18, for the lateral bladders 2 and 5, denoted as $p^{VI}_{c,left}$ and $p^{VI}_{c,right}$, respectively.

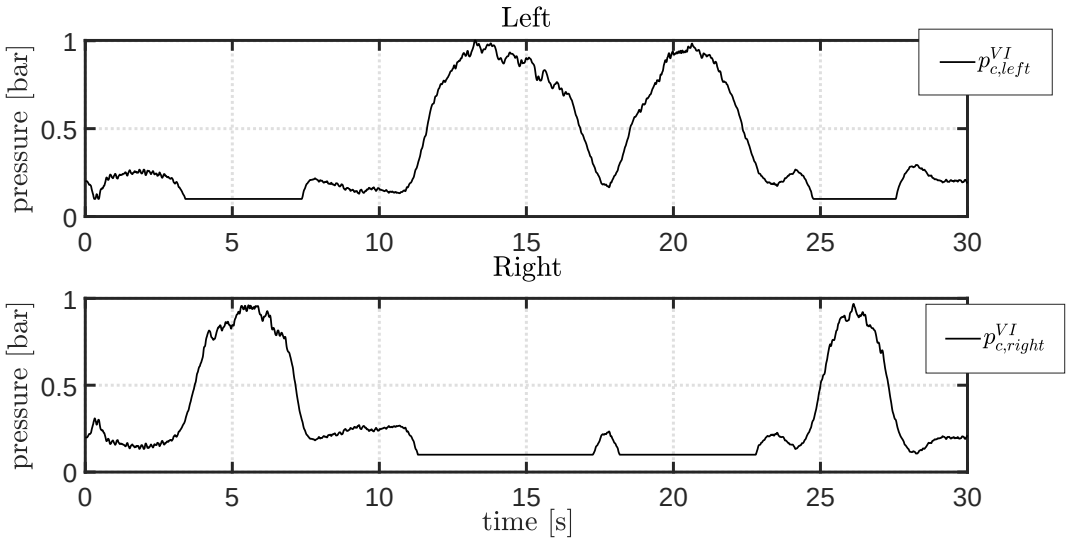

Figure 5.18: Output of the actual control system of section 2.2.

The enhanced version of the actual control, developed in section 4.2.1, computes the inner pressures $p^*_{c,left}$ and $p^*_{c,right}$, exploiting equation 4.6. The pressure induced by the simulator movement is computed using model 4.4 or 4.5. The overall control scheme is reported in figure 4.1. The contact pressure computed by the models is shown in figure 5.7, whether the

corresponding control outputs, $p_c^*(p_{lat}^*)$ and $p_c^*(\hat{p}_{lat})$, are reported in figure 5.19 The conversion gain V is set to $V = 10$, using a trial and error procedure. In figure 5.19, in the opening

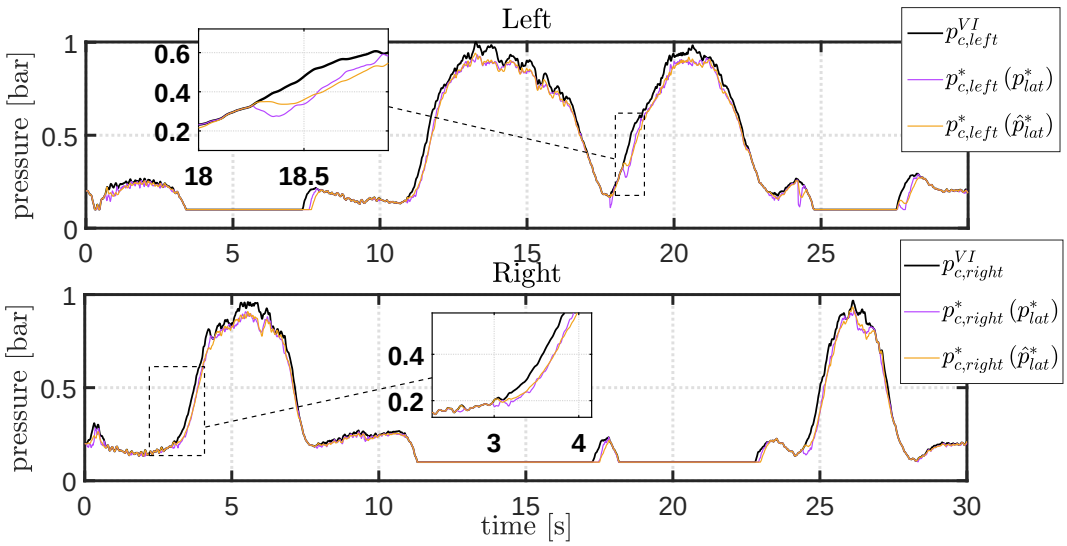

Figure 5.19: Comparison of the computed inner pressures of the bladders 2 and 5 of figure 2.1: $p_c^*(p_{lat}^*)$ (in purple) exploits the control scheme in figure 4.1 and model 4.4, $p_c^*(\hat{p}_{lat}^*)$ (in yellow) is computed with the control scheme in figure 4.1 and model 4.5, and p_c^{VI} (in black) is obtained with the actual control of section 2.2.

part of a turn, we can notice that the outputs of the enhanced control scheme, p_c^* are delayed with respect to p_c^{VI} . In these small intervals of time, the simulator platform movement creates a pressure on the driver, hence there are no need for the bladders to inflate. Instead, when the platform movement, limited by the physical constraints of the simulator, can not provide a sufficient pressure on the driver, the bladders are activated to sustain the pressure feeling. The inner pressures, $p_c^*(p_{lat}^*)$ and $p_c^*(\hat{p}_{lat}^*)$, are comparable. The small delay in the pressure computed using the filtered model 4.5 is not so remarkable. In the zoomed picture of the output pressure of the left bladder, is highlighted how delays in the movement of the platform, with respect to the real vehicle, can lead to peaks of pressure in the opening phase of a turn.

5.3.2 Feedforward control scheme

In section 3.2, a control scheme for the active seat system is introduced. This control scheme is adapted in section 4.2.2 for the realization of an haptic feedback, exploiting one of the lateral models among 4.4 and 4.5. The control system aims to transmit to the driver informa-

tion on the acceleration intensity and direction, taking into account the pressure induced by the simulator movement. In figures 5.6 and 5.7 are shown the contact pressures between the driver and the seat in the real car and in the simulator, respectively. Applying the Active seat compensation policy *Split&Splice*, described by equation 3.15, the desired contact pressure between the driver and the bladders p_0 is obtained, handling the possible inconsistencies between the two inputs. In figure 5.20, the desired contact pressures of the bladders, p_0^* and $\hat{p}_0^*$, are shown for both lateral models. From the desired contact pressure p_0, applying the

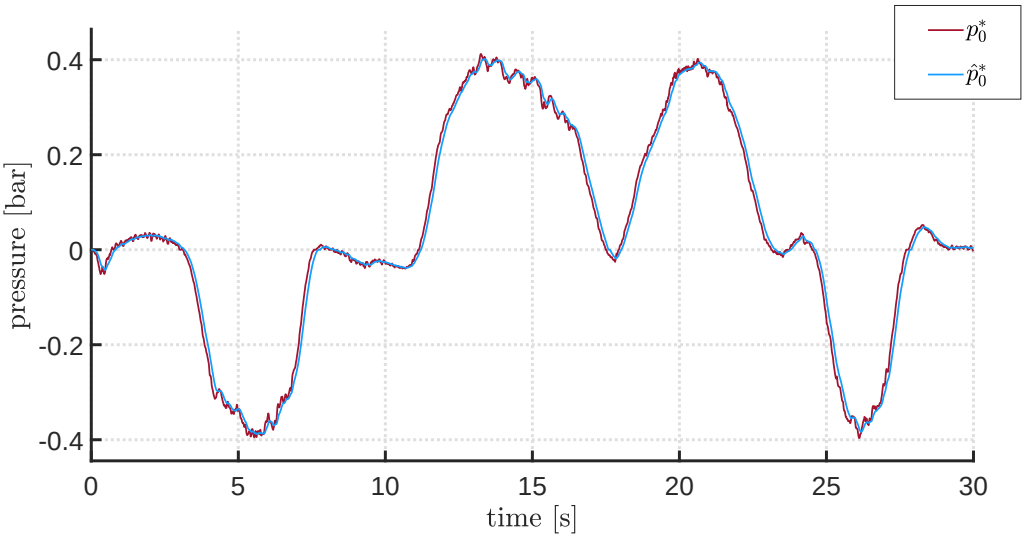

Figure 5.20: Comparison between the desired contact pressure of the bladders computed with different lateral models. p_0^* is computed starting from model 4.4, $\hat{p}_0^*$ starting from model 4.5.

inflatable bladder model of section 2.4, we can compute the inner pressure of the bladders, obtaining the results in figure 5.21. The computed inner pressure for both models, $p_c^{FF}(p_0^*)$ and $p_c^{FF}(\hat{p}_0^*)$, follows the same trend of p_c^{VI}. The computed pressure induced by the platform movement is quite small in the considered scenario but, nevertheless, the inflation of the bladders is slightly delayed, as can be seen in the zoomed picture in figure 5.21. The signals $p_c^{FF}(p_0^*)$ and $p_c^{FF}(\hat{p}_0^*)$ have an higher magnitude in the middle phase of a turn. This could be partially due to the parameters of the actual control, computing p_c^{VI}, since that particular behavior is obtained with a nonlinear gain.
Although the inflatable bladder model is the same of section 5.2.1, there is no body-tracking behavior of the bladders since the assumption of a driver integrated with the the seat.

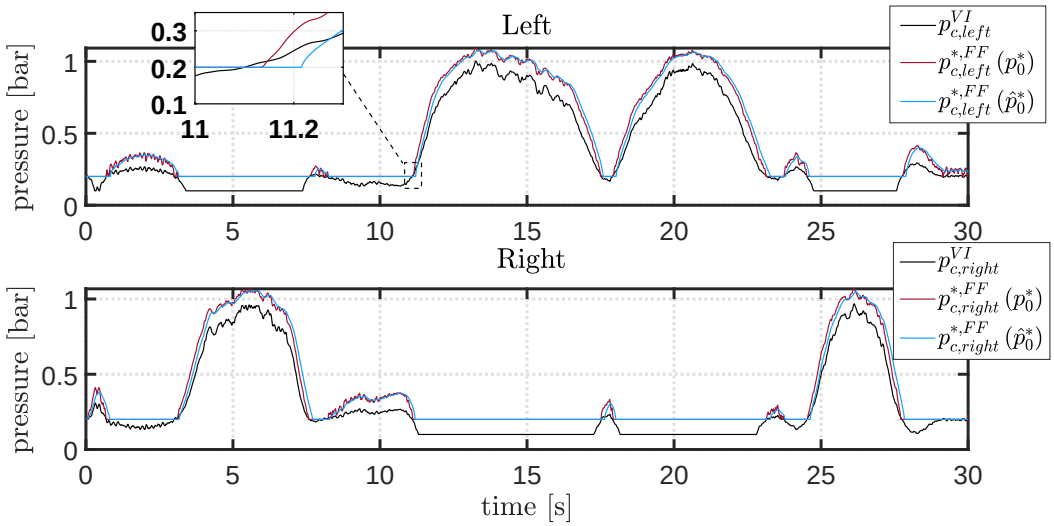

Figure 5.21: Outputs of the feedforward control for the realization of an haptic feedback. The red signal is obtained starting from model 4.4 and the light blue signal using model 4.5.

6

Conclusions and future work

Nowadays, the Active Seat system is used in simulators for the reproduction of the low-frequency acceleration that can not be recreated by the platform movement. Providing an artificial somatosensory stimulus, the driver's sensory system can be tricked to perceive an increased acceleration. This is possible since the human perception of motion is achieved integrating different stimuli from different sensory systems.
The open problem is how to compute the pressure cues to further enhance the driver's perception.
This thesis presents and develops two different control strategies for the active seat system in a dynamic driving simulator for a future implementation on a real platform. In these control strategies the pressure induced by the platform movement is taken into account.
The first control strategy considered, namely the model-based pressure cues approach, aims at reproducing the same pressure stimuli the driver would perceive in a real vehicle. To achieve this goal, a nonlinear model of a seated driver subject to acceleration is introduced. Both the feedforward control and the MPC scheme developed achieve good and comparable performance. The lateral bladders inflate and sustain the pressure cue when the platform movement can not provide sufficient pressure on the driver. The performance of these strategies are influenced by the precision of the driver's lateral model since the tracking behavior of the bladders requires a good estimation of the driver's trunk displacement.
For what is concerning the second approach, other two control schemes are proposed. These control schemes aim at creating an haptic feedback informative on the magnitude and the di-

rection of the acceleration the driver should perceive. The first one is an enhanced version of the actual control, while the second one is a feedforward control scheme. Both control schemes show promising results, delaying the activation of the bladders during the platform movement. The feedforward control slightly overestimates the inner pressure of the bladders with respect to the other models.

The natural development of this work is the implementation of these control schemes on a real dynamic simulator with a professional driver to identify which is the best control strategy to enhance the simulated driving experience.

A

Parameters values

Parameter	Symbol	Value	Measurement unit
Gravitational mass	M	50	$[Kg]$
Inertial mass	m	67	$[Kg]$
Height of the center of mass of the driver	h	0.45	$[m]$
Height of the driver	L	0.9	$[m]$
Contact area of a bladder	A	0.016	$[m^2]$
Backrest inclination	α	10	$[^\circ]$
De Wit model parameter	σ_0	10^4	
De Wit model parameter	σ_1	0	
Stribeck velocity	v_s	0.005	$[\frac{m}{s^2}]$
Nominal static friction value	F_s	45	$[N]$
Nominal dynamic friction value	F_d	30	$[N]$
Correction term for gravitational lateral component	K_{grav}	0.03	
Correction term for friction	K_{fric}	0.1	

Parameter	Symbol	Value	Measurement unit
Seat stiffness coefficient	k_2	3×10^6	
Intrinsic driver stiffness coefficient	k_0	100	
Seat damping coefficient	c_2	10^6	
Intrinsic driver damping coefficient	c_0	200	
Cut-off frequency of filter in model \ref{filtAccModel}	f_{fm}	62.8	$[Hz]$
Bladder radius before inflation	r_0	0.04	$[m]$
Bladder radius/inner pressure conversio gain	K_{bl}	10^7	
Elastic contact characteristic parameter	G	$0.17x10^8$	
Contact/Inner pressure gain	V	10	

References

[1] A. Berthoz, W. Bles, H. Bülthoff, B. Correia Grácio, P. Feenstra, N. Filliard, R. Huhne, A. Kemeny, M. Mayrhofer, M. Mulder, H. Nusseck, P. Pretto, G. Reymond, R. Schlusselberger, J. Schwandtner, H. Teufel, B. Vailleau, M. M. Van Paassen, M. Vidal, and M. Wentink, *Motion Scaling for High-Performance Driving Simulators*, 05 2013, vol. 43.

[2] M. Baseggio, A. Beghi, M. Bruschetta, F. Maran, and D. Minen, "An mpc approach to the design of motion cueing algorithms for driving simulators," 10 2011, pp. 692–697.

[3] A. Beghi, M. Bruschetta, and F. Maran, *A real time implementation of MPC based Motion Cueing strategy for driving simulators*, 12 2012.

[4] M. Bruschetta, F. Maran, and A. Beghi, "Nonlinear, mpc-based motion cueing algorithm for a high-performance, nine-dof dynamic simulator platform," *IEEE Transactions on Control Systems Technology*, vol. 25, pp. 1–9, 05 2016.

[5] M. Ernst and M. Banks, *Humans integrate visual and haptic information in a statistically optimal fashion*, 02 2002, vol. 415.

[6] M. Ernst and H. Bülthoff, *Merging the Senses into a Robust Percept*, 05 2004, vol. 8.

[7] M. Bruschetta, K. N. de Winkel, E. Mion, P. Pretto, A. Beghi, and H. Bülthoff, *Assessing the contribution of active somatosensory stimulation to motion perception in dynamic driving simulators*.

[8] VI-GRADE, *VI-DriveSim 18.1 Documentation*, 2018.

[9] G. Bisio, *Strategie di controllo per sedili attivi in simulatori dinamici di guida*. Università di Padova, AA 2018/2019.

[10] D. Cunico, *Motion Cueing algorithms for the integration of an active seat in a dynamic driving simulator*. Università di Padova, AA 2016/2017.

[11] T. W. Showalter and B. L. Parris, *The Effects of Motion and g-Seat Cues on Pilot Simulator Performance of Three Piloting Tasks*, 1980.

[12] J. Hamill, K. Knutzen, and T. Derrick, *Biomechanical basis of human movement*, 01 2014.

[13] C. Wit, H. Olsson, K. Åström, and P. Lischinsky, *A New Model for Control of Systems with Friction*, 04 1995, vol. 40.

[14] V. Popov, *Contact Mechanics and Friction: Physical Principles and Applications*, 01 2010, vol. 55.

[15] I. Muller and H. Struchtrup, *Inflating a Rubber Balloon*, 10 2002, vol. 7.

[16] M. Baseggio, *Generazione dei riferimenti per il Motion Cueing basato su MPC in simulatori dinamici di veicoli*. Università di Padova, 2011.

[17] M. Pozzi, *Motion Cueing per simulatori dinamici di veicolo: algoritmi MPC basati su modelli percettivi*. Università di Padova, 2011.

[18] R. Telban, W. Wu, F. Cardullo, and J. Houck, *Motion Cueing Algorithm Development: Initial Investigation and Redesign of the Algorithms*, 04 2000.

[19] G. Chung, W. Han, H. Kim, S. Chung, J. Park, C. Wallraven, and S.-P. Kim, *Adaptation of cortical activity to sustained pressure stimulation on the fingertip*, 2015.

[20] H. ten Donkelaar, A. Keyser, and P. van Domburg, *The Somatosensory System*, 05 2011.

[21] Y. Chen, *Algorithms and Applications for Nonlinear Model Predictive Control with Long Prediction Horizon*. Università di Padova, 2017.